## A Project report on

# A FIRST-PRINCIPLES STUDY ON THE IMPACT OF DOPING AND VACANCIES IN $\beta - Ga_2O_3$

Submitted in partial fulfillment of the requirements for the award of the degree of

**MASTER OF TECHNOLOGY** 

IN VLSI

**Submitted By** 

**GUNTU VARSHA GOPALKRISHNA** 

(186W1D5722)

Under the Esteemed Guidance of

Ms. J.MERINA M.Tech., Assistant Professor



# DEPARTMENT OF ELECTRONICS & COMMUNICATION ENGINEERING

#### ISTS WOMEN'S ENGINEERING COLLEGE

(Affiliated to Jawaharlal Nehru Technological University Kakinada, Kakinada)EAST GONAGUDEM, RAJANAGARAM, E. G. DIST, A.P-533294

#### ISTS WOMEN'S ENGINEERING COLLEGE

(Affiliated to Jawaharlal Nehru Technological University Kakinada, Kakinada)

#### **DEPARTMENT OF ELECTRONICS & COMMUNICATIONENGINEERING**



#### **CERTIFICATE**

This is to certify that Project report entitled "A FIRST-PRINCIPLES STUDY ON THE IMPACT OF DOPING AND VACANCIES IN B –GA2O3" is being submitted by GUNTU VARSHA GOPALKRISHNA (186W1D5722) in the partial fulfillment of the requirement for the award of the degree of Master of Technology in Electronics and Communication Engineering with specialization in VLSI during the academic period of 2019-2021.

## **Project Guide**

**Head of the Department** 

Ms. J.MERINA M.Tech.,

Prof.T.CHANDRA SEKHAR.,

**Assistant Professor** 

HOD

**EXTERNAL EXAMINER** 

#### **ACKNOWLEDGEMENT**

A Successful Project is a fruitful culmination of efforts by many people, some were directly involved, and some others quickly encouraged and supported from the background. I owe a great many thanks to a ISTS WOMEN'S ENGINEERING COLLEGE who helped and supported me during the accomplishment of the Project.

It is a great privilege for me to convey my sincere gratitude to DR. J.B.V. SUBRAMANYAM Principal of our college for his encouragement and for providing excellent lab facilities.

I would like to express my heartfelt thanks to Dr.Y. VENKAT Professor & Dean Academics of our college, for his encouragement and providing me with the necessary facilities to carry out this project.

I would like to express my sincere thanks to Dr.CH.VIJAYA KUMAR, Dean & R&D of our college, for his encouragement and providing me with the necessary facilities to carry out this project.

I would like to gratefully acknowledge our Head of the department of Electronics and Communication Engineering Prof.T.CHANDRA SEKHAR has been abundantly helpful and has assisted me in numerous ways.

I would like to express my sincere thanks to my Project guide Ms. J.MERINA for his valuable guidance, best suggestions and constant encouragement right to the inception to the end of this report which is also enabled to complete the Project successfully in time.

I wish to thank all the staff members in the department for their kind co-operation and my parents to give support throughout the Project work.

Finally I acknowledge sincerely the effective services rendered by one and all involved directly and indirectly in the entire Project.

GUNTU VARSHA GOPALKRISHNA (186W1D5722)

#### **DECLARATION**

#### I certify that

- a. The work contained in the thesis is original and has been done by me under the guidance of my supervisor.
- b. The work has not been submitted to any other institute for any other degree or diploma.
- c. I have followed the guidelines provided by the Institute in preparing the thesis.
- d. I have conformed to ethical norms and guidelines while writing the thesis.
- e. Whenever I have used materials (data, models, figures, and text) from other sources, I have given due credit to them by citing them in the text of the thesis and giving their details in the references.

Guntu Varsha Gopalkrishna (186W1D5722)

## **Abstract**

 $Ga_2O_3$  is a wide band gap semiconductor, allowing us to operate at larger voltages than its better-known competitors SiC and GaN. The project deals with first principle DFT based modelling and investigation on the performance by the impactof various structural phases, number of layers and impact of doping and impurities on  $Ga_2O_3$ . The advantage of using hybrid functions in the first principal calculations over the DFT based calculations is observed. Gallium oxide has low conductivity compared to other semiconductor devices due to its large band gap.

The electronic structure and optoelectronic properties of Nb-doped  $\theta$ -Ga2O3 were investigated by using plane wave ultrasoft pseudopotential generalized gradient approximation +U (GGA + U) method based on density functional theory. Four supercell models, namely, Ga23O36Nb1, Ga32O48, Ga39O6ONb1, and Ga47O72Nb1, were constructed. Results show that the formation energy of the doped system is lower and has higher stability under Ga-rich conditions than in O-rich conditions. With the increment in Nb doping concentration, the formation energy and lattice constant gradually increase, the stability of the system gradually decreases, and the band gap of the system gradually narrows. As the doping concentration increase, the absorption intensity increases.

In this project we try to analyze the ballistic conduction in the semiconductor channel. Ballistic transport means transport of carriers over long distances in the channel without any scattering. Lindauer's approach allows to analyze about transport of carriers in semiconductor materials. By using this approach, we can find the number of modes or channels contributing for current flow in the channel.

## **Abstract**

If many channels conduct, we get the maximum ballistic conduction which means the maximum current density of the device. The project analyses the variation of ballistic conductance by moving from bulk to 2D layers on  $\theta - Ga_2O_3$  and by different dopants on gallium oxide.

Furthermore, the increasing doping concentration accelerates the separation of holes and electrons, prolongs the carrier lifetime, and enhances conductivity. These conclusions provide a certain theoretical basis for the wide application of  $\theta$ -Ga2O3.

**Keywords**: Band gap, Density functional theory, Donors, Impurities, Current density.

## **Contents**

Ti	tle P	Page	i
Ce	ertifi	cate by the Supervisor	ii
D	eclar	ration	iii
Α¢	ckno	wledgement	iv
A	bstra	act	v
1	Intr	roduction	1
	1.1	Objective	2
	1.2	Thesis Organization	2
2	Lite	erature Survey	3
	2.1	Introduction	3
	2.2	High electric field breakdown and BFOM	3
	2.3	Ga <sub>2</sub> O <sub>3</sub> compared to other semiconductors	5
	2.4	Polymorphism and Crystal structure	5
		2.4.1 $\alpha - Ga_2O_3$	6
		2.4.2 $\beta - Ga_2O_3$	7
		2.4.3 Other polymorphs	8
3	DF	T based modelling	9
	3.1	Introduction	9
	3.2	Hartree-Fock approximation	10
	3.3	Electron density	10
	3.4	Kohn-Sham Equations	11
	3.5	Limitations of DFT	12
C	ITNC	ENTS vi	

4	Pro	posed Work	13
	4.1	Modelling layers	14
	4.2	Effective Mass	14
	4.3	Ballistic transport by Landauer's Formalism	15
	4.4	Doping and vacancies in $\beta$ – $Ga_2O_3$	19
5	Res	ults	21
6	Cor	nclusion and Future Scope	32
	Refe	erences	34

## **List of Abbreviations**

DFT Density functional theory

FOM Figure of Merit

GGA Generalized Gradient Approximation

BFOM Baliga Figure of Merit

WBG Wide Band gap

HSE Heyd-Scuseria-Ernzerhof

# **List of Figures**

2.1	Breakdown Field variation with Band gap	4
2.2	Properties of Ga <sub>2</sub> O <sub>3</sub> relative to some other major semiconductors	
	considering their different kinds of FOM	5
2.3	Crystal Structure of α – Ga <sub>2</sub> O <sub>3</sub>	6
2.4	Crystal Structure of β – Ga <sub>2</sub> O <sub>3</sub>	7
2.5	Different sites of Ga in $\beta$ – $Ga_2O_3$ . (a) Ga(I) of Tetrahedral and	
	(b) Ga(II) of Octahedral coordination	8
2.6	(c) Cubic lattice structure of $\gamma$ – $Ga_2O_3$ . (d) Orthorhombic $\varepsilon$ –	
	Ga <sub>2</sub> O <sub>3</sub> structure	8
4.1	Conductor between the two contacts	15
4.2	E vs k diagram for different transverse modes	18
5.1	Crystal Structure of β – Ga <sub>2</sub> O <sub>3</sub>	21
5.2	Unit cell of $\theta$ – $Ga_2O_3$	22
5.3	Crystal structures of Monolayer and Bilayer of $\beta$ – $Ga_2O_3$	22
5.4	Geometrical structures of layers of $\beta$ – $Ga_2O_3$	23
5.5	Side view of layers	24
5.6	Band Structure of bulk $\theta$ – $Ga_2O_3$	24
5.7	Band structures of layers	25
5.8	Oxygen vacancies in $\beta$ – $Ga_2O_3$	

# **List of Figures**

5.9	Band structures due to oxygen vacancies in $\beta - Ga_2O_3$	. 27
5.10	Band structures due to gallium vacancies in $\beta$ – $Ga_2O_3$	. 27
5.11	Doping in $\beta - Ga_2O_3$	. 28
5.12	Band structures of different dopants in $\theta - Ga_2O_3$	. 29
5.13	Conductance variation with energy in $\beta$ – $Ga_2O_3$ layers	. 30
5.14	G variation with Energy for different concentration of doping in $oldsymbol{ heta}$	
	– $Ga_2O_3$ . For (a) 3% (b) 15% (c) 25% doping concentration in Si, Ge,	
	Sn and (d)3% (e)15% doping concentration for deep donors	
	Ir and Cr	31

# **List of Tables**

5.1	Band gaps	23
	Comparison Table	
	Band gap due to vacancies	
5.4	Band gap	28

## Introduction

Gallium oxide  $(Ga_2O_3)$  is evolving as a feasible candidate for certain classes of power electronics and opto-electronics, due to its ultra-large band gap (4.4-4.9eV). Photo detectors based on  $Ga_2O_3$  have the cutoff wavelength range of 250–280nm, which meets the requirements for detection over a deep ultra-violet (DUV) region and can be seen as an emerging star in the field of solar-blind UV photo detectors.

The theoretical critical field strength ( $E_c$ ) of  $Ga_2O_3$  is 8 MV/cm and value of Baliga figure of merit (BFOM) is over 3000, which is very high than other WBG semiconductors like GaN, SiC [1]. This makes it as a promising candidate in future power electronic applications. There are 5 polymorphs of  $Ga_2O_3$ , namely  $\alpha$ ,  $\beta$ , $\gamma$ , $\delta$  and  $\varepsilon$ .

Among which, the monoclinic ( $\theta$ ) phase of  $Ga_2O_3$  denotes the most stable, most widely studied and utilized phase[1, 3]. The project deals with the first principles study on the structure and electronic properties of this  $\theta - Ga_2O_3$ . Although it has high breakdown voltage and high band gap, but it has an intrinsic mobility which is less than GaN and SiC [4].

It also gives a low hole mobility which makes it difficult to get p-type conductivity. Many theories have shown that 2D materials performance are dependent on their thickness. Therefore, we look forward in this project on how performance of gallium oxide can be improved by moving to 2D  $\theta$  –  $Ga_2O_3$  layers and effect of different dopants on bulk gallium oxide.

Gallium oxide has been of interest for certain classes of power electronics and optoelectronics (solar blind UV detectors, photodetectors etc.) due to its ultra-large bandgap (4.4- 4.9 eV).

The band gap and breakdown field strength are related exponentially by the universal equation  $E_c$ =  $a(E_g)^n$ , where a and n have fixed values for direct and indirect material.

- So a small increase in bandgap increases breakdown field largely.
- BFOM also depends on the electric field strength and given by BFOM =  $\mu \epsilon E_c^{-3}$ .

Because of high bandgap and high BFOM, it is better than other WBG semiconductors like SiC, GaN.

Diamond and AIN have higher bandgaps than gallium oxide but advantageous in terms of low cost.

Advantages of high-quality crystalline films, and lower  $R_{on}$  resistance because of high  $E_c$  and has low conductivity compared to SiC, GaN and difficulty in p-type conduction.

## 1.1 Objective

The project aim is to achieve the following:

- A study on the optimal conditions for generating maximum ballistic drive current in  $\beta$   $Ga_2O_3$  FETs.
- Study on the impact of doping and vacancies in  $\theta$   $Ga_2O_3$ .

## 1.2 Thesis Organization

Organization of the report is as follows:

**Chapter 2** describes a brief literature survey on the background, crystal structure and different phases of gallium oxide.

**Chapter 3** focuses on DFT based modelling, Hybrid functionals.

Chapter 4 describes about the proposed work.

**Chapter 5** presents the results that have been produced by the proposed implementation.

**Chapter 6** concludes the thesis by giving the conclusion and future direction related to this project.

## **Literature Survey**

#### 2.1 Introduction

For high power electronic applications, we need materials which can sustain at high temperatures and voltages. Wide band semiconductors are useful for this type of applications and so are preferred over narrow band semiconductors.

Si has bandgap Eg = 1.1eV and 0.65eV for Ge. So, Si was considered the WBG semiconductor at the time and this was one of the key reasons for Si's growth in replacing Ge as the original semiconductor.

Later, group III (e.g. GaN, AIN) and group IV materials (e.g. SiC, diamond) have been introduced extending the band gap range to well over 4eV. Gallium oxide belongs to group III oxides and is an emerging WBG semiconductor with its properties of interest [1].

### 2.2 High electric field breakdown and BFOM

The electric field in the depletion region of semiconductors can become extremely high when a high voltage is applied. Even in a pure semiconductor, current willflow when the applied electric field reaches the critical value *Ec*, then system will have experience electrical breakdown ultimately failure of device.

So, the amount of electricity required to convert an insulator to a conductor is called the Breakdown voltage (*Ec*). The breakdown voltage determines how much power the device can handle. The higher the breakdown voltage, more power the device can handle.

The band gap of the semiconductor is related to the electrical breakdown value. The graph obtained by using this condition as shown in Fig. 2.1 and we can observe the theoretical value breakdown field of around 8MV/cm assuming the band gap of  $Ga_2O_3$  as 4.9eV[1, 18]. From the figure we can observe, the breakdown field for diamond is around 10MV/cm indicating Diamond has more band gap than  $Ga_2O_3$ .

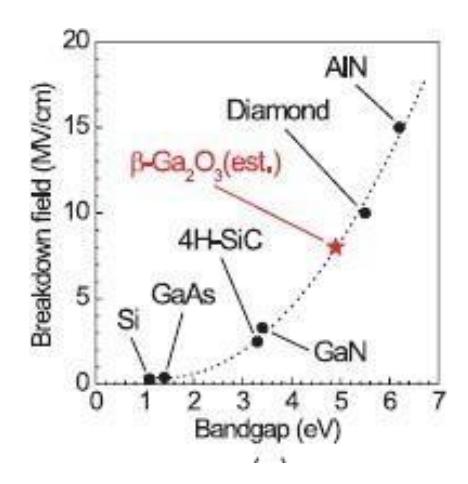


Figure 2.1: Breakdown Field variation with Band gap

The universal relationship that can be used for finding the breakdown voltage is in the form of  $E_c = a$  ( $E_G$ )<sup>n</sup> with the coefficient a and index n (a and n have a fixed values for direct and indirect materials) [17]. The band gap and breakdown field strength are related exponentially, so small increase in band gap increases the Breakdown field strength largely.

For the output of power semiconductor devices, several FOM (Figure of Merit) methods have been defined which are helpful to identify the device performance. High FOM numbers indicate good performance of devices. One such metric is proposed by Baliga, is the Baliga figure of merit (BFOM) which indicates minimizing conduction losses. Higher the value less will be the losses.

## 2.3 $Ga_2O_3$ compared to other semicondutors

Throughout the history of semiconductors in the field of microelectronics, researchers have increasingly favored semiconductors with wider bandgaps. The increasing demand for semiconductor devices has continued this trend to find more suitable materials, and Ga2O3 is currently considered a possible candidate. In 1952, the polymorphs of Ga2O3 had already been reported and its rich material systems with potentially excellent properties were considered ideally suitable for modern electronic applications

With a bandgap of more than eV, Ga2O3 conforms the instinct advantages of ultra-wide-bandgap semiconductors. It has a better breakdown electric field, a higher temperature tolerance, and better resistance to radiation than the current third-generation semiconductors. Coupled with an excellent Baliga's figure-of-merit (BFOM), all these characteristics are necessary for high-power applications in electronic devices. In addition, such a wide bandgap can also ensure a low leakage and offer great potential for deep-ultraviolet (DUV) detection, placing Ga2O3 in a uniquely important position in the field of optoelectronic devices.

This review firstly focuses on the bulk growth of Ga2O3. We introduce the remaining problems of Ga2O3 growth, including volatilization, decomposition, crucible corrosion, and strong anisotropy; and the mainstream growth methods, including float-zone (FZ), Czochralski (CZ), edge-defined film-fed growth (EFG), and vertical Bridgman (VB) methods. It provides an exhaustive analysis of the epitaxy of Ga2O3 films as another pivotal procedure in the application process. Compared with wide-bandgap semiconductors such as GaN and AlN, for epitaxy,  $\theta$ -Ga2O3 offers a large wafer size, low cost, and high availability using halide vapor phase epitaxy (HVPE), molecular beam epitaxy (MBE), metal-organic chemical vapor deposition (MOCVD), and pulsed laser deposition (PLD), atomic layer deposition (ALD) methods. It discusses the defects and interfaces of Ga2O3, which particularly affect the material property and device performance.

#### **2.3** $Ga_2O_3$ compared to other semicondutors

Other large band gap semiconductors such as GaN and SiC are currently in use. However, how do we decide the right technology to invest in? We're particularly interested in  $Ga_2O_3$  because of its large band gap and high electric breakdown field strength as compared to other materials as seen from Table 2.2 [1, 4].

Material Parameter	Si	GaAs	4H-SiC	GaN	Diamond	β-Ga <sub>2</sub> O <sub>3</sub>
Bandgap $E_g$ (eV)	1.14	1.43	3.25	3.4	5.5	4.8
Dielectric constant ε	12	13	10	9	5.5	11
Breakdown field $E_{C}$ (MV/cm)	0.3	0.4	2.5	3.3	10	8
Carrier mobility $\mu$ (cm <sup>2</sup> /(V·s))	1450	8400	1000	1200	2000	300
Saturation velocity $v_{sat}$ (10 <sup>7</sup> cm/s)	1	1.2	2	2.5	1	2
Thermal conductivity K (W/mK)	150	50	370	250	2000	10-30
FOM relative to Si						
Baliga FOM = $\varepsilon \mu E_c^3$	1	14.7	317	846	24 660	3200
$Johnson FOM = E_c^2 v_{sat}^2 / 4\pi^2$	1.	1.8	278	1089	1110	2844
Baliga High Frequency FOM = $\mu E_c^2$	1	10	46	100	1500	142
Keyes FOM = $\kappa[(cv_{sat})(4\pi\epsilon)]^{1/2}$	1	0.3	3.6	1.8	41.5	0.2

Figure 2.2: Properties of  $Ga_2O_3$  relative to some other major semiconductors considering their different kinds of FOM

The high breakdown field of gallium oxide as discussed in Section 2.1 compared to others, shows its applications in high voltage and high power devices like aircrafts, solar cells etc. High BFOM indicating minimal losses as discussed in Section 2.1. Seeing from the table Diamond and AIN are better than gallium oxide but gallium oxide is advantageous from them in terms of low cost. All otherFOMs except Keyes FOM[1] of  $Ga_2O_3$  is significantly higher than that of SiC and GaN because of its very low thermal conductivity. So, gallium oxide has been in interest for high voltage applications.

### 2.4 Polymorphism and Crystal structure

Polymorphs are different crystal forms of the same compound, differing due to the arrangements of molecules within the unit cells of the crystalline lattice of each crystal form. Overall the contents of the crystals are the same, as can be judged by HPLC, GC (for any solvated solvents), elemental analysis, KF titration, and other assays. Different polymorphs may display different physical properties, such as solubility, melting points, heats of fusion upon melting, density, hardness, crystal shape, and stability to moisture and light. Crystals containing a solvated solvent are sometimes referred to as polymorphs but are more appropriately termed pseudo polymorphs.

The presence of solvents can be inferred by thermogravimetric analysis (TGA) as small weight losses near the boiling points of the solvent, and can be confirmed by GC, NMR, and other analyses. (Solvents may be lost from solids at temperatures above the boiling points: the strength of hydrogen bonds between a solvent and an API or excipient may be different than that of hydrogen bonding of one solvent molecule to another.

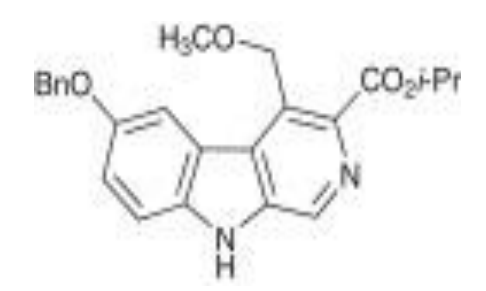
Solvents that are stoichiometric with the API will be present at concentrations higher than those allowed for residual solvents unless the solvent in question is H2O (as a hydrate). Hydrates are crystals containing water of solvation. If an anhydrous form is present, it may be referred to as an anhydrate. Other types of solids are desolated solvates, brittle solids from which residual solvents in crystal lattice were removed by drying, and amorphous solids, which display no crystalline content .

The FDA definition of polymorphs includes not only crystalline anhydrates, hydrates, and solvates, but also amorphous forms .Most drug substances are crystalline solids, primarily because APIs can be upgraded by crystallization during manufacturing, and because crystalline solids often display bulk stability superior to that of amorphous solids. Good bulk stability of the drug substance will usually confer good shelf life of the drug product.

In a drug product, a change in the morphic state of the API can alter the ease of formulation, the rate of tablet dissolution, the solubility and bioavailability of API, and the shelf life. Changes in the appearance of the drug product, such as tablets that disintegrate upon storage or crystals growing through walls of gel-caps, can affect patient compliance with the medication. In 1969 Halebian and McCone discussed the impact of polymorphs on various formulations and recommended that pharmaceutical companies thoroughly investigate polymorphism in APIs. They also recommended that the most stable polymorph be developed.

#### **2.3** $Ga_2O_3$ compared to other semicondutors

Two examples serve to illustrate the importance of understanding polymorphism. Crystallization of abecarnil which became a problem when Form B, the least stable of three known polymorphs, could no longer be crystallized on scale.



Process improvements had generated API batches of higher potency, and key impurities were no longer present to help template the formation of Form B. The goal became to make Form A without contamination by Form C, the most stable polymorph. One scale-up solution was to generate Form B by spray drying, which affords another example of Ostwald's rule of crystallization by stages. Subsequent laboratory developments found the optimal processing was to use clean A as seeds, activate the seeds by slurring in solvent before charging to solution, charge 3 wt.% seeds at proper concentration and temperature, and cool at 0.5–1.0 °C/minute (rapid cooling on scale) to prevent crystallization of Form C.

Critical to the success of these operations on scale was rapidly removing the mother liquor by loading a centrifuge to a wet cake thickness of only 1 cm and centrifuging; these steps prevented rapid solvent-mediated transformation. The detail required for these procedures, which are certainly creative and feasible, point out the desirability of selecting the most stable polymorph as the API.

#### 2.3 <u>Ga<sub>2</sub>O<sub>3</sub> compared to other semicondutors</u>

The same chemical composition but with different molecular packing of crystalline materials are termed as polymorphs. These are the 5 different polymorphs possible for  $Ga_2O_3$  [20, 21], which are known as  $\alpha$ ,  $\beta$ ,  $\gamma$ ,  $\delta$  and  $\varepsilon$ .

```
Rhombohedral phase (\alpha - Ga_2O_3)
Monoclinic phase (\beta - Ga_2O_3)
```

```
Defective spinel phase (\gamma - Ga_2O_3)
Cubic phase (\delta - Ga_2O_3)
Hexagonal phase (\varepsilon - Ga_2O_3)
```

 $\beta$  –  $Ga_2O_3$  is the most stable polymorph compared to other polymorphs which is widely used and studied. The project also deals with monoclinic phase  $\beta$  –  $Ga_2O_3[1]$ .

#### 2.4 Polymorphism and Crystal structure

#### $\alpha$ , $\theta$ and $\gamma$ -Ga2O3

 $\alpha$ ,  $\beta$  and  $\gamma$ -Ga2O3 have been successfully obtained in an easily scalable synthesis using aqueous solution of gallium nitrate and sodium carbonate as starting materials without any surfactant and additive.  $\alpha$  and  $\beta$ -Ga2O3 were obtained by calcination at 350 and 700 °C, respectively, of  $\alpha$ -GaOOH, prepared by controlled precipitation at constant pH 6 and T = 55 °C, with 24 h of aging.

Aging was necessary to fully convert the initially precipitated gel into a well-crystalline and phase-pure material.  $\gamma$ -Ga2O3 was obtained after calcination at 500 °C of Gallia gel, synthesized at constant pH 4 and T = 25 °C, without aging. These three polymorphs have a for Gallia relatively high surface area: 55 m2/g ( $\alpha$ -Ga2O3), 23 m2/g ( $\beta$ Ga2O3) and 116 m2/g ( $\gamma$ -Ga2O3). The combination of X-ray diffraction (XRD), scanning electron microscopy (SEM), energy dispersive X-ray analysis (EDX), nitrogen physisorption and thermogravimetry (TG) was employed to characterize the samples and their formation.

#### Introduction:

Gallium oxide is widely used for the preparation of gas sensors, optoelectronic devices, luminescent materials and catalysts in diverse gas and liquid phase chemical reactions. It is an insulator with a wide band gap at room temperature (~4.9 eV for  $\beta$ -Ga2O3), which is considered to be the widest band gap semiconductor among transparent conducting oxides (TCOs) [12-14]. However, preparation of  $\beta$ -Ga2O3 under reducing conditions or heating in reducing atmospheres at high temperature turns it into an n-type semiconductor.

For example, a substantial conductivity increase was observed for  $\beta$ -Ga2O3 crystals, when grown under reducing conditions in an inductive couple's plasma torch. This increase could be quenched again upon annealing in oxygen, indicating that oxygen vacancies are the source of the enhanced conductivity Such vacancies act as shallow donors and their role on the luminescence properties of  $\beta$ -Ga2O3 has been studied in detail by Binet and Gorier.

#### 2.4 Polymorphism and Crystal structure

Gallium oxide is also used as a catalyst support, in particular for Pd-based catalysts. In such systems, the partial reduction of Gallium may lead to the formation of Ga-Pd intermetallic compounds, which have interesting properties in methanol synthesis, methanol steam reforming and hydrogenation reactions A large specific surface area of nanostructured gallium oxide is desired for both applications as gas sensor and catalyst.

Five modifications of Ga2O3 are known:  $\alpha$ ,  $\beta$ ,  $\gamma$ ,  $\delta$  and  $\epsilon$  and a thermodynamic description of the system Ga-O has been presented. Among these five modifications,  $\beta$ Ga2O3 is the most stable modification (mp 1740 °C); it has a monoclinic structure with the oxide ions in distorted ccp arrangement and Gallium oxide in distorted tetrahedral and octahedral sites.  $\alpha$ -Ga2O3 crystallizes in the structure of corundum. It forms upon heating of  $\alpha$ - 4 Gao OH in air between 450 and 550 °C. It also has been reported by Remeika and Marezio that single crystals of  $\alpha$ -Ga2O3 have been grown from a flux at a pressure of 44 kbar and at a temperature of 1000 °C.

γ-Ga2O3 is assumed as a cubic spinel-type structure Bohm has described the preparation of this Gallia polymorph and found a crystal structure similar to that of γ-Al2O3. Zinkevich et al. found differences in the cation distribution between both compounds and discuss the similarity of γ-Ga2O3 with η-Al2O3. Areán and Delgado have reported that γ-Ga2O3 was prepared by calcination (at 500 °C) of a Gallia gel obtained by adding ammonia to an ethanolic solution of gallium nitrate. They attributed the presence of excess water in Gallia gels to the formation of a product, probably Gao OH, which is not a precursor of γ-Ga2O3 but rather of the  $\alpha$ -Ga2O3 polymorph. Hence, they advised to avoid the use of water as a solvent when preparing γ-Ga2O3  $\delta$ -Ga2O3 crystallizes like In2O3 in the C-type structure of rare earths.

It can be prepared by heating the residual of evaporated gallium nitrate solution at 200-250 °C. When it is heated above 500 °C, the  $\delta$  modification transforms to orthorhombic  $\epsilon$ -Ga2O3 [28]. In summary, the polymorphism of Ga2O3 is very similar to that of Al2O3:  $\alpha$ -,  $\beta$ -,  $\gamma$ - and  $\epsilon$ -Ga2O3 are isomorphous with  $\alpha$ -,  $\theta$ -,  $\gamma$ - or  $\eta$ - and  $\kappa$ -Al2O3, respectively, but there is no form of Al2O3 that corresponds to  $\delta$ -Ga2O3 [27]. In the present work, we have investigated a simple aqueous chemistry route to synthesize precursors of Ga2O3, and showed that not only  $\alpha$ -,  $\beta$ -, but also  $\gamma$ -Ga2O3 can be formed by thermal treatment of precursors obtained from aqueous solution. The detailed characterization work, effect of different synthesis parameters like pH and temperature, will be discussed.

#### **2.4.1** $\alpha - Ga_2O_3$

In each unit cell, there will be six formula units of gallium oxide, with two separates lattice parameters "a" and "c" with values of 4.98Å and 13.43Å, respectively [1, 22]. The Ga ions occupy oxygen two-thirds of the octahedral sites and oxygen ions are closely packed in a hexagonal pattern as shown in Fig 2.3[1, 4].

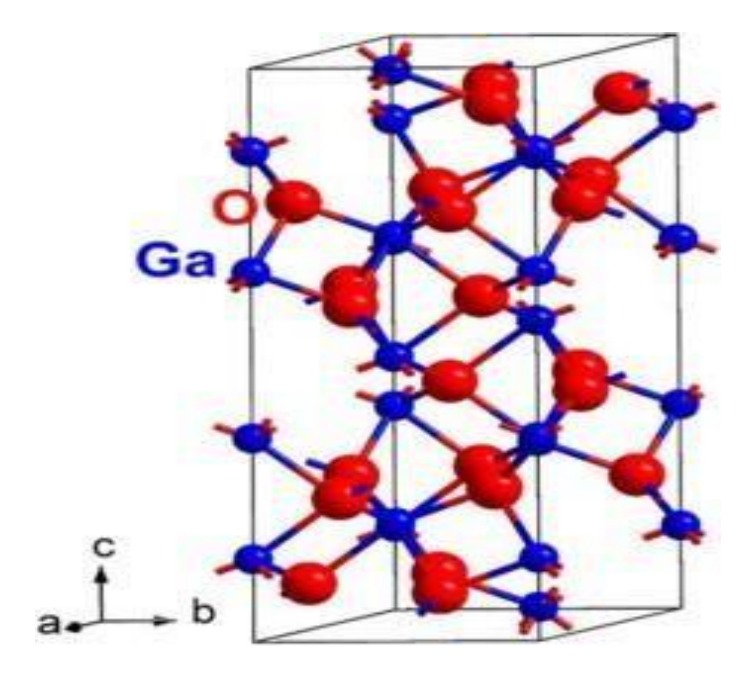


Figure 2.3: Crystal Structure of  $\alpha - Ga_2O_3$ 

One of the important properties of  $\alpha - Ga_2O_3$  is, its band gap is around 5eV, which is higher compared to all other polymorphs of  $Ga_2O_3$ . Few other values were calculated [23, 24] all of which came out to be around 5eV. Since our interest is in wide band gap materials, we can consider this polymorph of gallium oxide. But $\alpha - Ga_2O_3$  is meta-stable and at high temperatures around 750–900°C it converts to more stable  $\theta - Ga_2O_3$ , so which makes it difficult to prepare bulk crystals of  $\alpha - Ga_2O_3$ .

#### 2.4 Polymorphism and Crystal structure

#### **2.4.2** $\theta - Ga_2O_3$

This phase of  $Ga_2O_3$  is key subject of the project and more details of its properties will be discussed here.  $\theta - Ga_2O_3$  has a base-centric monoclinic crystal structure, belongs to space group C2/m, as shown in Fig 2.4[1, 4].

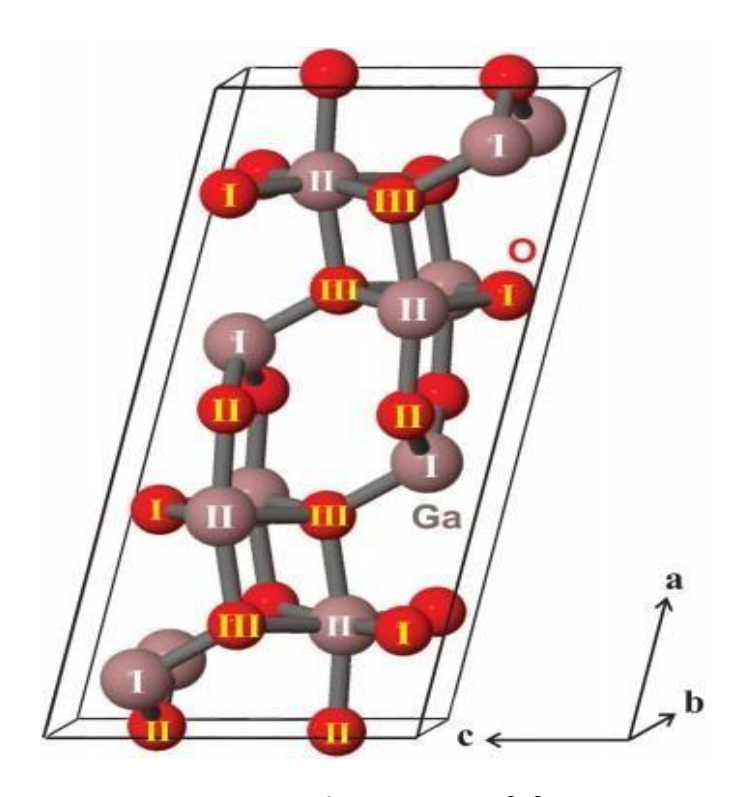


Figure 2.4: Crystal Structure of  $\theta - Ga_2O_3$ 

The lattice parameters [3] are a = 12.21 Ű, b = 3.04 Å, c = 5.80 Å.  $\alpha$ ,  $\beta$ ,  $\gamma$  are the angles between b and c axes, c and a axes, a and b axes respectively. For monoclinic,  $\alpha = \gamma = 90^{\circ}$  and  $\theta = 103.8^{\circ}[2]$ .

There are two different Ga sites, labeled Ga(I) and Ga (II). The Ga(I) atoms in tetrahedral arrangement are bonded to the four adjacent O atoms. The Ga (II) atoms bind to six neighboring O atoms in an octahedral environment.

#### 2.4 Polymorphism and Crystal structure

The O atoms have three distinct sites: O(I) and O(II) bonded to three Ga atoms whereas the O(III) binds to four Ga atoms shown in Fig 2.5[1, 4]. The different position of Ga and O atoms leads to an anisotropic behavior, which means different optical and electrical properties along different planes.

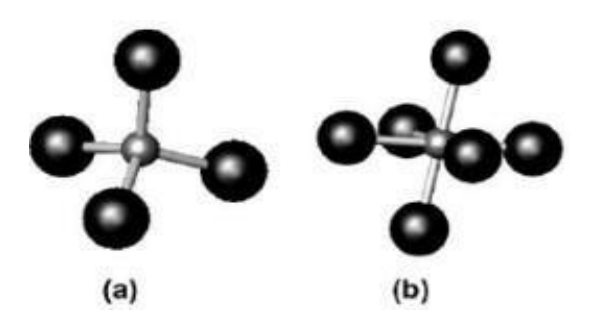


Figure 2.5: Different sites of Ga in  $\theta$  –  $Ga_2O_3$ . (a) Ga(I) of Tetrahedral and (b) Ga(II) of Octahedral coordination

#### 2.4.3 $\alpha$ - and $\beta$ -Ga2O3 Formation

The XRD patterns of the  $\alpha$ -Gao OH precursor, after treatment at different calcination temperatures,  $\alpha$ -Gao OH is still the only phase after calcination at 300 °C for 2 h, which is in agreement with the observation that  $\alpha$ -Gao OH is stable up to 300 °C. The lattice constants have slightly decreased compared to the dried precursor (a = 9.7885(2) Å, b = 2.9730(1) Å, c = 4.5197(2) Å supporting the idea that crystal water removal occurs as the first step of calcination. The XRD pattern of the sample after calcination at 350 °C for 2 h is different and can be identified as the rhombohedral phase of Gallia,  $\alpha$ -Ga2O3 (R –3c). 4c and the experimentally determined lattice parameters are a = 4.9873(3) Å and c = 13.450(1) Å, which is in good agreement with literature values (a = 4.9825(5) Å, c = 13.433(1) Å.

When the calcination temperature exceeds 700 °C, the material is transformed to the monoclinic polymorph (C2/m) of Gallia,  $\beta$ -Ga2O3. The experimental lattice parameters are a = 12.288(1) Å, b = 3.0364(3) Å, c = 5.8085(5) Å,  $\beta$  = 103.78(1)  $^{\circ}$  and similar to the previously reported values of a = 12.214(3) Å, b = 3.0371(9) Å, c = 5.7981(9) Å,  $\beta$  = 103.83(2)  $^{\circ}$  . A graphical representation of the Rietveld fit is shown in Fig. 4d. The calcination behavior of  $\alpha$ -Gao OH can be also followed by SEM micrographs. Through d show the surface morphology of spindle-like particles after calcination for 2 h in air at 350, 650, 700 and 950 °C, respectively. The initial shape and size of the aggregates are basically conserved during the phase transformation from  $\alpha$ -GaOOH to  $\alpha$ -Ga2O3 and then to  $\beta$ -Ga2O3, but the platelet-like shape of the primary particle gradually fades as the calcination temperature is increased. In addition, nano-sized pores appear on their surfaces and are enlarged as calcination temperature is increased. Table 1 summarizes textural properties of the gallium oxide hydroxide and gallium oxides obtained after calcination.

The adsorption-desorption isotherm of nitrogen and pore size distribution curve are shown in Fig. 8. All isotherms are typical for mesoporous materials containing micropores. The fact that the hysteresis loop moves to a higher relative pressure as the calcination temperature increases suggests that the most frequent pores are wider for  $\beta\text{-Ga2O3}$  than for  $\alpha\text{-Ga2O3}$ .

#### 2.4 Polymorphism and Crystal structure

The pore size distribution was analyzed following the BJH method applied to the desorption branch of the isotherm. In most cases, a very narrow maximum at d = 4 nm is observed. Such sharp signal was not found in the pore size distribution derived from the adsorption branch, which is exemplified. Thus, the maximum at 4 nm is 11 not reflecting the porous properties of the material, but rather identified as the so-called tensile strength effect phenomenon, an artifact due to the forced closure of the hysteresis loop with a sudden drop of the isotherm along the desorption branch in the p/po range 0.41-0.48, which was described in detail by Groen et al.

For this study, desorption data is used for the particle size distribution, which is considered more accurate compared to adsorption data, and the signal at d = 4 nm is ignored in the analysis. Thus, the real pore size distributions of the Gallia materials show a broader maximum at pore diameters between 3 and 18 nm (Fig. 8, insets). While the loss of surface area with higher calcination temperature (with the exception of the transformation to  $\beta$ -Ga2O3, Table 1) suggests considerable sintering and particle growth, we cannot find growth and coalescence of particles in the SEM images (Fig. 7). Thus, these phenomenon's could be explained by the decreasing number and widening of the original pores inside the original aggregates, which gives rise to a shift of the broad peak in the pore size distribution with calcinations temperature from 5 to 18 nm (Fig. 8a-d, insets). Tas et al. reported that in a loose powder compact the crystals fused together at their mutual point of contact after calcination at 1200 °C for 6 h [1].

Summarizing this part, treatment at relatively low temperature results in  $\alpha$ -Ga2O3 with relatively high surface area of 55 m2 g-1 and pores of a diameter of ca. 10 nm. As the calcination temperature is increased, the pores widen and specific surface area decreases without significant change of the aggregate sizes. A similar behavior is observed for  $\beta$ -Ga2O3, which can be obtained with 23 m2 g-1 and 25 nm-pores. Thus, phase-pure  $\alpha$ - and  $\beta$ -Ga2O3 with relatively large surface area and high pore volume can be produced by calcination of  $\alpha$ GaOOH at 350 and 700 °C in air for 2 h, respectively.

### 2.4.4 Other polymorphs

There is no enough information available or done about the next three polymorphs and they not are widely used. The  $\varepsilon$  –  $Ga_2O_3$  crystal structure is not well understood also[1]. These three crystal structures are also metastable and convert to  $\beta$  –  $Ga_2O_3$  at high temperatures Fig 2.6[1, 2].

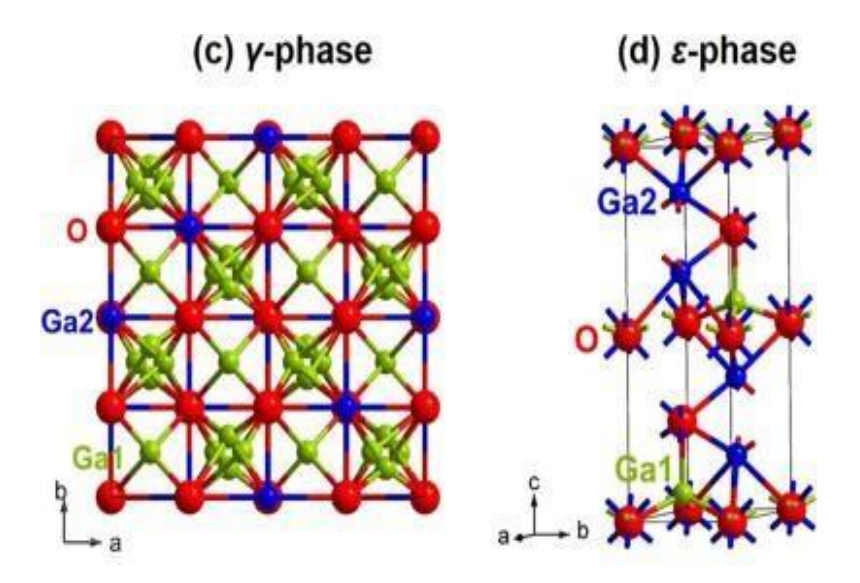


Figure 2.6: (c) Cubic lattice structure of  $\gamma$  —  $Ga_2O_3$  . (d) Orthorhombic  $\varepsilon$  –  $Ga_2O_3$  structure.

## **DFT** based modelling

#### 3.1 Introduction

For calculating the electronic structure and properties of atoms, crystals, surfaces, and their interactions the most commonly used method is the Density functional theory (DFT). In quantum mechanics the main problem we want to solve are all about involving atoms and molecules. For any system of a non-trivial size, it is difficult to find a quantum solution [5]. So the main focus of DFT theory is to replace many electrons wave function to a simple entity.

To obtain the properties of interest of a many body system we need to have an approximate solution of time independent Schrodinger equation. Furthermore, the Born-Oppenheimer approximation which is widely used, ignores the nuclei motion and allows the total energy of the electrons in the potential provided by the nuclei has to be calculated[5]. As a result, the below equation can be used to determine the total electronic energy in the ground state (lowest energy configuration), as

$$\hat{H}\psi(x_1, x_2, x_3, .... x_N) = E\psi(x_1, x_2, x_3, .... x_N)$$
(3.1)

where  $\hat{\mathbf{H}}$  is the Hamiltonian operator of the system (sum of potential and

#### 3.2 Hartree-Fock approximation

kinetic energy),  $\psi$  is a many-electron wave function of the N-electron system, E is total electron energy. Since we need a approximate solution for Eq 3.2 various approximation methods are used mentioned below.

### 3.2 Hartree-Fock approximation

The Hartree–Fock (HF) method is an approximation method for determining a quantum many-body system wave function and energy in a stationary state. It is assumed that a single Slater determinant [4, 5, 26] will approximate the system's exact N-body wave function.

One can derive a set of N-coupled equations for the N spin orbitals by using the variational method. The Hartree–Fock wave functionand the system's energy are obtained by solving these equations[4]. However, the problem with these approaches is that they require a lot of computation effort, which makes it difficult to apply them to more complex systems efficiently.

## 3.3 Electron density

In two famous and essential theorems (Hohenberg and Kohn 1964, Kohn and Sham 1965)[5, 26, 27] which gives an alternative theoretical formulation for determining the electronic structure was demonstrated as that the total energy of a solid (or atom) can be expressed uniquely as a functional of the electron density. So, order to determine the ground-state capacity, we can minimise this functional with re- spect to density.

As a result, rather than using a many-electron wave function,  $\psi(x_1, x_2, x_3, ....x_N)$  so the ground-state energy can be expressed in terms of the electron density at a single point n(r), where that density is due to all the electrons in the solid[5]. The probability of having a single electron with a spin S1 amongN electrons in the volume element ds1 is given by the electron density n(r), while the rest of the wave functions have arbitrary spin and position.

$$\int \int \int n(r) = N \dots |\psi(x_1, x_2, x_3, ....x_N)|^2 ds_1 dx_2 dx_3 ... dx_N$$
 (3.2)

The pure (or orbital-free) DFT attempts to compute the energy of interacting electrons, as a functional of the density. Although this method is right in theory, it is not very reliable in practise and yields very few electronic properties values.

This is due to the kinetic energy functions lack of precise approximations. Kohn and Sham (1965) proposed an alternative approach in order to overcome this problem, Instead of using the many-electron wave function to calculate the electron density,  $\psi(x_1, x_2, x_3, x_N)$  can be used to solve efficient one-electron problems.

## 3.4 Kohn-Sham Equations

The Kohn–Sham equation is the one-electron Schrodinger equation of an atomic system of non-interacting particles that generate the same density as any given system of interacting particles. The trick is to find an efficient potential  $V_{eff(x)}$  for one-electron states using the form of the total-energy functional, and then solve for the one-electron states to get a density equal to the many-electron density. The one-electron states have the following equation [5]:

$$\left(-\frac{\mathrm{k}^2\nabla^2}{2m} + V_{eff}(r)\right)\phi_i = \varepsilon_i\phi_i \tag{3.3}$$

where  $\varepsilon_i$  is the orbital energy of the corresponding Kohn–Sham orbital  $\phi_i$ . The charge density of the N-electron system can also be expressed as a function of the number of non-interacting one-electron Kohn-sham orbitals:

$$\rho(x) = \sum_{i=1}^{2} |\phi_i|^2 \tag{3.4}$$

The power of Kohn-sham method is that choosing an effective potential  $V_{eff}(x)$  such that  $n(r) = \rho(r)$ .

The Kohn-sham approximation now gives the total energy of the interaction system using charge density by Eqn 3.5

$$E[\rho(r)] = T[\rho] + J[\rho] + E_{XC}[\rho] + E_{ne}[\rho]$$
 (3.5)

where  $J(\rho)$  represents columbic effects,  $E_{XC}(\rho)$  corresponds to exchange energy, external potential acting on the interacting system.  $T(\rho)$  represents the kinetic energy of the effective of one-electron,  $E_{ne}(\rho)$  is the electron-nuclei interaction. The major contribution of the energy is exchange correlation energy. The Kohnsham equation is not based on any approximation and gives exact ground state energy provided the exact  $E_{XC}$  exchange correlation functions are known.

#### 3.5 Limitations of DFT

Density functional approaches can be divided into three categories. The local density approximation (LDA) [28] method - assumes that the molecule density is uniform all around the molecule and relies solely on the value of the electronic density at each point in space, which is generally not a useful method.

The Generalized Gradient Approximation (GGA)[29] method - tries to correct of the non-uniformity of the electron density, and the Hybrid Functional Methods method tries to account for the non-uniformity of the electron density[29]. The precision of DFT lies in the accuracy of the DFT method which is used to approximate the  $E_{XC}$  exchange correlation functions.

It was discovered that hybrid functions try to combine some of the more useful features of ab initio methods (specifically Hartree-Fock methods) with some of the improvements of DFT mathematics. There are many widely used hybrid functions such as LDA+U, GGA+U, B3LYP, HSE06 etc. But the use of hybrid functions are costly since it requires more time and more high computational access like access to supercomputers.

The long time because of less approximations compared to DFT, it is generally fastbut does not yield accurate results. For eg: HSE06 method requires 16 cores and minimum 30-40 minutes for a simulation, whereas a normal PC has 4-6 cores. So you will require high computing access for improved accuracy of electronic parameters. If you have limited computational resources or a small number of atoms analysis of materials by DFT is best and widely used with LDA or GGA methods.

# **Proposed Work**

The calculations for the project were performed based on density functional theory (DFT), as implemented in the Quantum Espresso package (QE). The input was modelled using a GUI called BURAI. The projector augmented wave (PAW) pseudopotential [11] is used. This pseudopotential is more reliable and precise than other ultra-soft pseudopotentials in handling complicated and complex situations, such as strong magnetic moments and large electronegativity variations [12].

The use of the PAW pseudopotentials addresses the problem of inadequate description of the wave functions in the core region common to other pseudopotential approaches [3]. The generalized gradient approximation (GGA) parameterized by PerdewBurkeErnzerhof (PBE)[12] was used as the exchange-correction functional. The convergence criterions were  $1 \times 10^{-6}$  eV for the self-consistent field energy.

The residual forces on each atom are 0.01 eV/Å. Vacuum of 15 Å is added perpendicular to the layer planes to reduce artificial interlayer interactions under the periodic boundary condition of  $\theta - Ga_2O_3[8]$ . To guarantee the accuracy of energy level descriptions in this project, the HSE06 hybrid functional[14] is used throughout this work.

The properties of bulk and 2D  $\theta$  –  $Ga_2O_3$  materials with different thicknessare studied here. For the bulk  $\theta$  –  $Ga_2O_3$ , the lattice parameters taken as a = 12.21 Å, b = 3.04 Å, c = 5.80 Å and with  $\theta$  = 103.8, which are in good agreement with proven experimental and theoretical values[3].

Since the lattice parameters and lengths of Ga-O bonds in the (100) direction are larger than those in the other directions, we can understand the exfoliation energy[10] of layers  $\theta - Ga_2O_3$  along the (100) surface is lower than that along the (010) and (001) surfaces.

This supports from the experimental findings that layers of  $\theta - Ga_2O_3$  are easier to obtain or cleave from the (100) surfaces of its bulk than other planes. So, the monolayer, bilayer, and trilayer are cleaved along (100) surface from bulk of  $\theta - Ga_2O_3$  [7] and the 2D  $\theta - Ga_2O_3$  layers are modelled and simulated as shownin Fig 5.3.

### 4.1 Modelling layers

Theoretically, Van de Wall [9] tried to model the monolayer  $\theta - Ga_2O_3$  structure by reducing the thickness of the monoclinic  $\theta - Ga_2O_3$  unit cell along the [100] direction down to half. Until now, some progress has been made based on this model[7]. The smallest step size on the (100) surfaces was measured to be half the conventional unit cell height, indicating that this is the smallest possible layer thickness of 2D  $\theta - Ga_2O_3$ [9].

A crystalline solid consists of repeating patterns of its components in three dimensions as shown in Fig 5.1, we can represent the entire crystal by drawing the structure of the smallest identical units that, when stacked together, form the crystal. This basic repeating unit is called a unit cell like as shown in Fig 5.1.

We can simulate like the shown figure with super cells which increases the computation effort with improved accuracy. Similarly for the layers as shown in Fig 5.3 we can have a super cell-repetition of unit cell in possible directions, or we can simulate with the unit cells as shown in Fig 5.4.

#### 4.2 Effective Mass

The effective mass of electrons and holes in a band is important for the transport property and also for describing various electrical properties of the material. Themass of a particle in vacuum is not the same as in a crystal because of its sur- rounding particles. Effective mass is the mass that a particle seems to have when it is interacting with other particles. The effective mass of a semiconductor is

obtained by fitting the actual E-k diagram around the conduction band minimum for electrons and the valence band maximum for holes by a parabola, like the above equation [16]

$$E(k) = E_C + \frac{k^2 k^2}{2m^*}$$
 (4.1)

$$\frac{1}{m^*} = \frac{1}{m^*} \frac{\partial^2 E}{\partial k^2} \tag{4.2}$$

where E(k) is the energy of an electron at wave vector k in that band,  $E_C$  is a constant giving the edge of energy of that band, and m\* is a constant (the effective mass). After the parabola fitting, we will get the equation of the parabola as in Eq 4.1, where  $m^*$  is a constant in that equation. Then after double differentiation of Eq 4.1 and divided by the square of reduced planks constant as in Eq 4.2 we get the effective mass.

## 4.3 Ballistic transport by Landauer's Formalism

Transport of carriers over long distances in the channel without any scattering is termed as ballistic transport. That means electrons travel at high speeds since no scatterings. When the mean free path of the travelling particle is longer than the dimension of the medium, then ballistic transport is observed. A general approach for understanding conduction properties or the ballistic transport Landauer's Formalism is used[25].

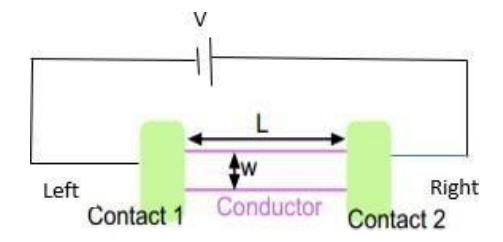


Figure 4.1: Conductor between the two contacts

Assume the channel is ballistic and connected between the two contacts  $\mu L$  and  $\mu_R$  with an equilibrium fermi energy level at  $\mu_o$  and no voltage is applied.

When apositive potential(V) is applied between left and right contacts the quasi fermi energy shift  $\mu_0$  from its equilibrium position given as

$$\mu_L = \mu_o + \Delta \mu_L, \, \mu_R = \mu_o - \Delta \mu_R \tag{4.3}$$

where  $\Delta\mu_L + \Delta\mu_R = qV$ , and the probability of occupancy of energy levels E is

$$f_{L}(E) = \frac{1}{1 + e^{(\frac{E - \mu_{L}}{L})}} f_{R}(E) = \frac{1}{1 + e^{(\frac{E - \mu_{R}}{L})}}$$
(4.4)

The flux of electrons entering the channel from left and right contact is given by

$$\frac{I_L(E)}{E} = D (E)f (E)v(E) = \frac{2}{2}f (E)$$
 (4.5)

$$\frac{I_R(E)}{q} = D (E)f(E)v(E) = \frac{h^L}{4}(E)$$
(4.6)

where  $D_{-}(E)$ ,  $D_{+}(E)$  are the density of states of electrons in channel, v(E) is the group velocity. Since the currents are flowing in opposite directions, total current given as

$$I(E) = I_L(E) - I_R(E)$$
 (4.7)

$$I(E) = \frac{2q}{-(f_L(E) - f_R(E))}$$
 (4.8)

$$I(E) = \frac{2q}{h} \frac{\partial f}{\partial E} qV \tag{4.10}$$

by neglecting the higher order terms in the Taylors expansion yields Eq 4.9

$$G = \frac{I}{2} = \frac{2q^2 \int_{-\infty}^{\infty} (-\frac{\partial f}{\partial E}) dE$$

$$V = h_{0} = \partial E$$
(4.11)

In the above equation if we assume the band edge starts from E = 0,

$$G = \frac{I}{V} = \frac{2q^2}{h} [-f(E_{\infty}) + f(E_0)]$$
 (4.12)

$$G = \frac{I}{V} = \frac{2q^2}{h} [f(E_0)] \tag{4.13}$$

If the fermi energy is deep inside the band then  $f(E_0) = 1$  giving the conductance value known as quantum conductance.

$$G_{max} = \frac{I}{V} = \frac{2q}{\frac{2}{h}}$$
 (4.14)

This is the maximum conductance of a nanowire like structure in the ballistic limit[27]. So, if we make the thickness of conductor shorter and shorter the conductance is not going to jump to infinity but reach a maximum value Eq 4.14. Now if there are some sources of scattering which inhibits the maximum flow of electrons Eq 4.12

$$G = \frac{2q^2 \int_{0}^{\infty} T(E)(-\frac{\partial f}{\partial E}) dE$$
 (4.15)

where T is the transmission probability and 1-T is the reflection probability. Transmission probability is the probability that an electron entering from left contact reach right contact. A ballistic conductor is an ideal transmitting conductor without any scatterers, indicating transmission probability of T = 1.

Transverse modes are the discrete channels in a narrow conductor, through which electronic transport takes place. The larger the conductor the greater number of transverse modes or channels. The effectively current carrying states are the states between  $\mu_L$ ,  $\mu_R$ .

The total number of transverse momentums states whose minimum energy lies below the energy  $E^{I}$  are the number of modes M(E) at energy  $E^{I}$ . With the cut-off energy  $E^{I}$  for each transverse mode n, means the bands above  $E^{I}$  does not contribute to conduction, only bands below  $E^{I}$  contribute to conduction and are given by M(E)-total number of modes available for conductionwhere M(E) per unit area can be found by

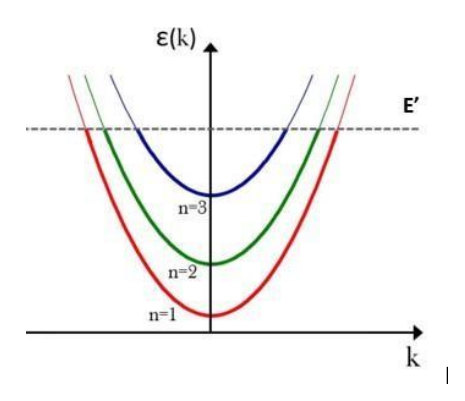


Figure 4.2: E vs k diagram for different transverse modes

$$M(E^{\dagger}) = \int_{0}^{E^{\dagger}} D(E) dE$$
 (4.16)

So for parabolic energy bands, the number of modes of 1D, 2D and 3D conductors are given by

 $M(E^{I}) = M_{1D}$  the number of modes below E'.

$$M(E^{I}) = WM_{2D}(E^{I}) = W \int_{0}^{E^{I}} \frac{\int_{E^{I}} \frac{1}{2m^{*}}}{D_{1D}(E) dE} = W \int_{0}^{E^{I}} \frac{1}{\pi k} \frac{2m^{*}}{E} dE$$
 (4.17)

(4.18)

$$M(E^{J}) = WM_{2D}(E^{J}) = WM_{2D}(E)_{J} = \frac{\sqrt{W23m*EJ}}{\pi k}$$

where W is the width of 2D conductor.

$$\int_{E'} \int_{E'} m^* dE$$

$$M(E^{I}) = AM_{3D}(E^{I}) = A \int_{0}^{\infty} D_{2D}(E) dE = A \int_{0}^{\infty} \pi k^2 dE$$

$$m^* E^{I}$$
(4.19)

$$(E^{I}) = A_{-}$$
 $M(E^{I}) = AM_{3D}$  (4.20)

where A is the area of 3D conductor. The generalized conductance equation which can be used is given below

$$G = \frac{I}{e} = \frac{2q^2 \int_{-\infty}^{\infty} M(E)T(E)(-\frac{\partial f}{\partial E}) dE$$

$$V = \frac{1}{e} \frac{2q^2 \int_{-\infty}^{\infty} M(E)T(E)(-\frac{\partial f}{\partial E}) dE$$

$$(4.21)$$

If the conductor is within the ballistic limit then T(E) = 1, which indicates the length of the conductor should be in the order of nanometers [7, 34] to observe ballistic conduction. If the conductor is longer than mean free path then transmission probability is T(E) at energy E. So here the final conductance equation is given by:

$$G = \frac{1}{V} = \frac{2q}{h} M(E)$$
 (4.22)

Using this equation, we can find the number of modes from band structure for 3D and 2D conductors assuming the conductor is within the ballistic limits. These calculations are done at zero bias and room temperature. Higher the values of ballistic conductance, even at more will be the current density even at a smaller voltage for short channel conductors.

## 4.4 Doping and vacancies in $\beta - Ga_2O_3$

Doping of semiconductors which is termed as introducing impurities to generate free carriers or valence electrons which can increase the conductivity of semiconductors. Addition of impurities can be intentional – doped on purpose or un- intentional – may be lack of control on the growth of semiconductor. When a high- energy particle, such as a proton, knocks an atom out of its lattice, it creates vacancies. The vacancies and impurities can be termed as defects and defects introduce new electronic levels in the band gap, which we can observe form the band structures which affects the electronic properties of devices.

If the new levels introduced by the donor or acceptor are close to the conduction-band minimum or valence-band maximum respectively then it is a shallow donor. That means the additional energy levels are not more than 1eV thermal energy (at room temperature) [32] away from the lower conduction band edge which is called the ionization energy.

If they have larger ionization energy then they are deep lev-els or traps which act as active recombination centers and annihilate each other, so there will not be much increase in conductivity. The original semiconductor has unaltered electronic properties if we use shallow dopants, making the impurity atoms only affecting the electron concentration.

Gallium acts like an insulator because of its ultra large band gap(4.9eV). A few different impurities have been anticipated to be effective n-type dopants in  $\theta$  –  $Ga_2O_3[31]$ . Silicon, germanium, tin, chlorine and fluorine of group IV and Iridium and chromium have also been investigated as likely donor dopants in $\theta$  –  $Ga_2O_3$ . Both fluorine and chlorine were found to be donors when substituting on the oxygen site [33].

Gallium oxide has 2 different sites for gallium and 3 different types of oxygen.

The project deals with mostly preferred n-type dopants of Group IV elements suchas Si, Ge and Sn substituting on the Ga site [2]. These donors may behave as n-type because they have one more valence electron than group-III Ga. This extra electron can be thermally accelerated to the CB, resulting in an n-type crystal. It has been shown that Si and Ge prefer the tetrahedral coordination of the Ga(I) site, while Sn prefers the octahedral coordination of the Ga(II) site [3] in Fig 5.11. Ir, Cr belong to transition elements(metals) and can exhibit variable valency.

Chromium can exhibit valency +3 or +2 and Iridium can exhibit +4 or +3. Here we have considered  $Ir^{+4}$  and  $Cr^{+3}$  and both prefer the Ga(II) +3 site as n-type donors. We know that there are 3 sites possible for oxygen vacancies O(I), O(II), O(III) in Fig 2.4. In  $\theta - Ga_2O_3$ , gallium vacancies ( $V_{Ga}$ ) are common defects. A missing Ga atom leaves three O dangling bonds that can accept electrons since Ga has three valence electrons. As a result,  $V_{Ga}$  serves as a triple acceptor.

The Ga(I) vacancy has been shown to have a lower formation energy than Ga(II)[2]. These all dopants can be used for doping in bulk crystals but it is difficult to dope 2D materials because since the size is very small it will be challenging to create vacancies or dope with impurities. For all these the ballistic conduction as a function of energy graphs are plotted.

Many theories have proven that[32], in  $\beta - Ga_2O_3$  or any other wide band gap semiconductors, it is impossible or very difficult to achieve p-type conductivity because of strong self-localization of holes[35]. When doped with Iron, Magnesium, Calcium[3] it was observed it creates deep donors resulted in deep acceptor levels, not being able to contribute to the p-type conductivity of  $\beta - Ga_2O_3$ [30] even with higher concentration of dopants. The experimental work on p-type doping of  $\beta - Ga_2O_3$  are very low in number.

## **Results**

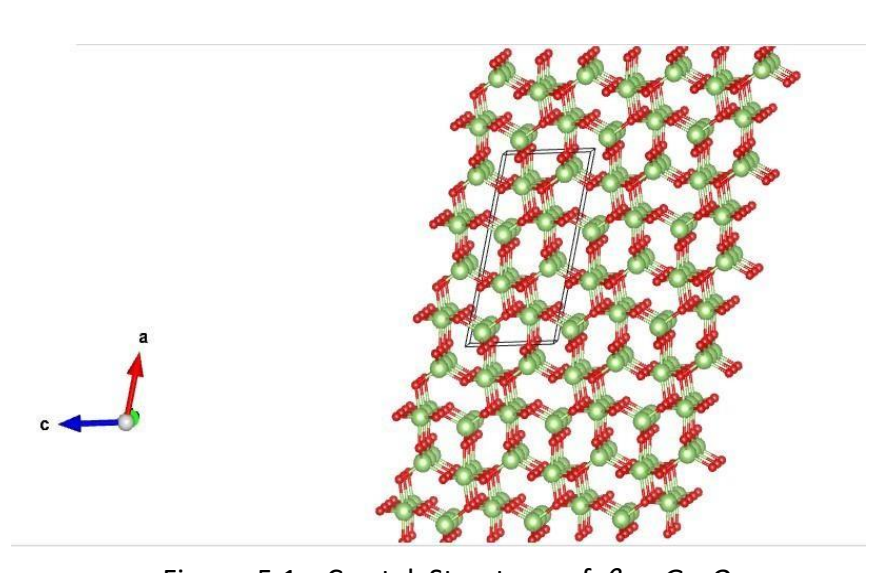


Figure 5.1: Crystal Structure of  $\theta - Ga_2O_3$ 

A unit cell when repeated in all the three dimensions gives us a crystalline solid. The above Fig 5.1 is the crystal lattice structure of  $\theta - Ga_2O_3$ . The box representing in the lattice is the unit cell of  $\theta - Ga_2O_3$  as shown in Fig 5.2. Aunit cell possess same properties as of bulk since it is the repeating unit. So whenwe give a unit cell of a material, what the DFT engine solves is a repetition of

the unit cell in all the three directions, which basically means that it simulates bulk Fig 5.1. So we can simulate a unit cell for the finding electronic properties or create super cells for more improved accuracy. As discussed in the modelling layers section, the crystal structure is cleaved along (100) surface plane for getting 2D materials which are shown in Fig5.3.

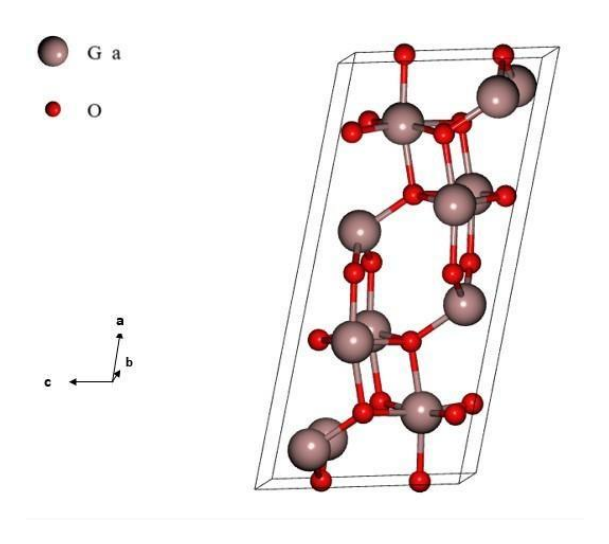


Figure 5.2: Unit cell of  $\theta - Ga_2O_3$ 

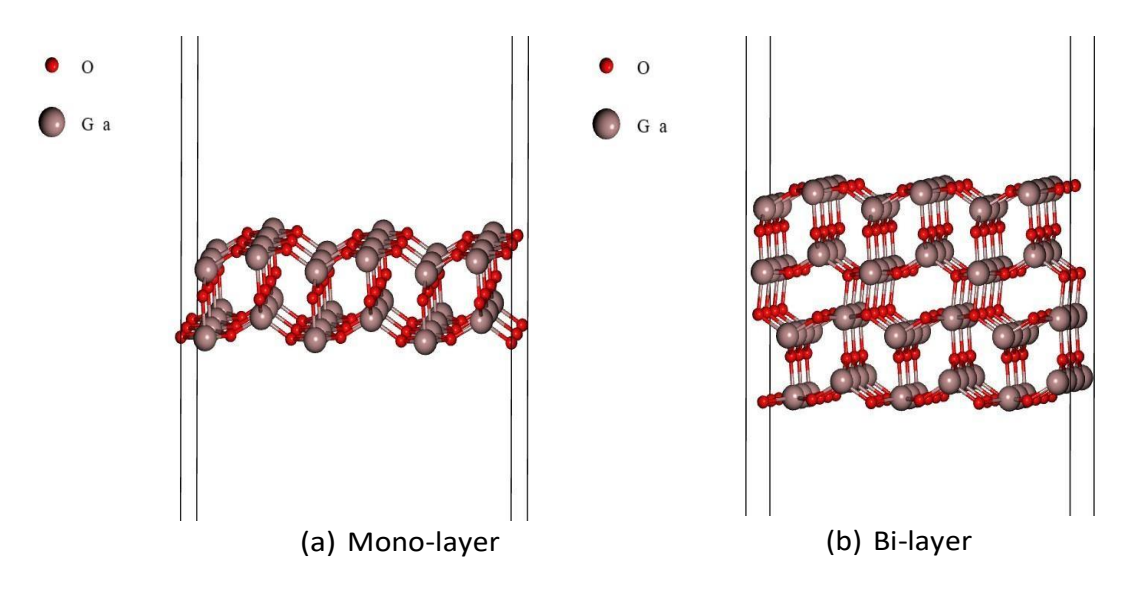


Figure 5.3: Crystal structures of Monolayer and Bilayer of  $\theta$  –  $Ga_2O_3$ 

Monolayer as mentioned, is reduced to half of the unit cell size with mini-mum possible layer thickness[9]. When moving from mono to bi means placing a monolayer on top of other gives bilayer similarly placing another layer on bilayer gives trilayer and so on to get the bulk as shown in Fig 5.4. Defining a primitive lattice in reciprocal gives Brillouin zone. k-points are the sampling points in the first brillouin zone. Brillouin zones are used to describe and analyze the electronenergy in energy band structure of crystals.

By the DFT calculations, the obtained electronic Band structure of  $\theta$  – $Ga_2O_3$  the E vs k along the high symmetric points Z- $\Gamma$ - A-M-L [4] are shown in Fig 5.6. From Figure we can observe the conduction band minimum and valence band maximum are at different momentum indicating a gallium oxide as an indirect semiconductor of band gap 4.8453eV with  $\Gamma$  centered origin in the band structure.

From the band structure of bulk  $\theta$  – $Ga_2O_3$ , The conduction-band minimum is located at the  $\Gamma$  point, while the valence-band maximum is located off  $\Gamma$ , we can say it is an indirect semiconductor whose calculated value of B.G = 4.84eV in acceptance with the theoretical values[7].

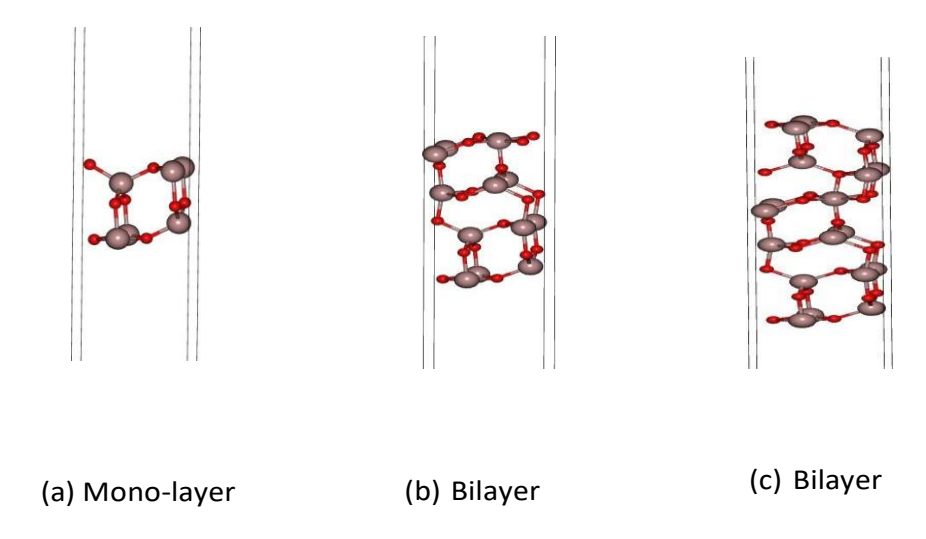


Figure 5.4: Geometrical structures of layers of  $\beta$  –  $Ga_2O_3$ 

The accuracy in the value of band gap is obtained by hybrid functional HSE06, giving a value of 4.8453eV of  $\theta$ - $Ga_2O_3$  in acceptance with the experimental values. The side view of bulk and layers along a and b directions are shown in Fig 5.5.

Table 5.1: Band gaps

	Band gap by	Band gap by
	DFT (eV)	using HSE06 (eV)
Bulk $\theta$ – $Ga_2O_3$	2.027	4.8453
monolayer	3.1256	5.6241
bilayer	2.678	5.238
trilayer	2.1207	5.128

The effective mass of electrons and holes in terms of mass of electron  $m_0$  obtained from the band structure as given by Eq 4.1. The bulk gallium oxide is isotropic. But the asymmetric positions of Ga and O atoms in 2D layers, it exhibits anisotropic nature. The Z- $\Gamma$ ,  $\Gamma$ - A of reciprocal lattice actually indicates the two different directions of crystal with k = 0 as origin at the  $\Gamma$  point in the reciprocal plane.

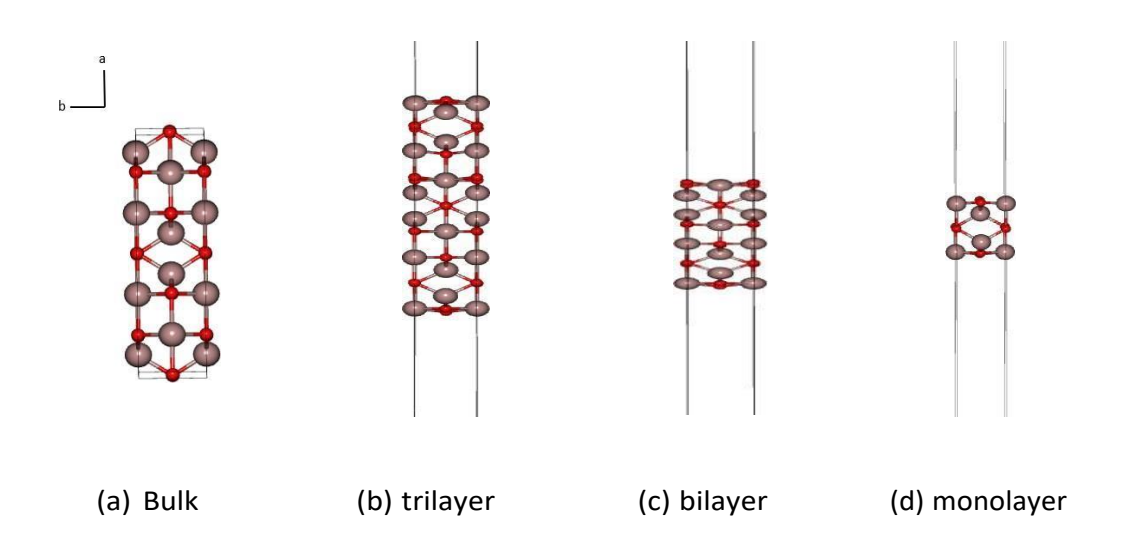


Figure 5.5: Side view of layers

Since the cleavage is along (100) plane, when indicated in the reciprocal lattice the  $\Gamma$ - A direction in corresponds to axis c and Z- $\Gamma$  direction corresponds to axis b [29] and the calculated effective mass along these directions shown in below Table 5.2. The effective masses along  $\Gamma$ - A are significantly larger than that along Z- $\Gamma$  because of asymmetric parabola for conduction band and theflatness of band near the valence band.

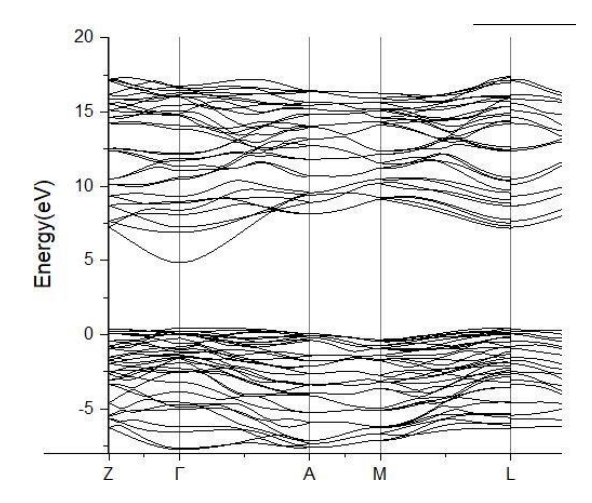


Figure 5.6: Band Structure of bulk  $\theta - Ga_2O_3$ 

We can observe the band gap variation of 2D materials with bulk crystal[7]. The layer dependent band gap can is due to quantum confinement in gallium oxide[15]. Gallium oxide is advantageous in terms of this layer dependent band gap which are stable also compared to other semiconductor materials.

Monolayer has higher band gap compared to others because of quantum confinement effect and since the thickness is small the atoms are tightly packed and it becomes difficult to excitean electron into the conduction band, so large energy is required. So, it is difficult to dope the 2D material practically.

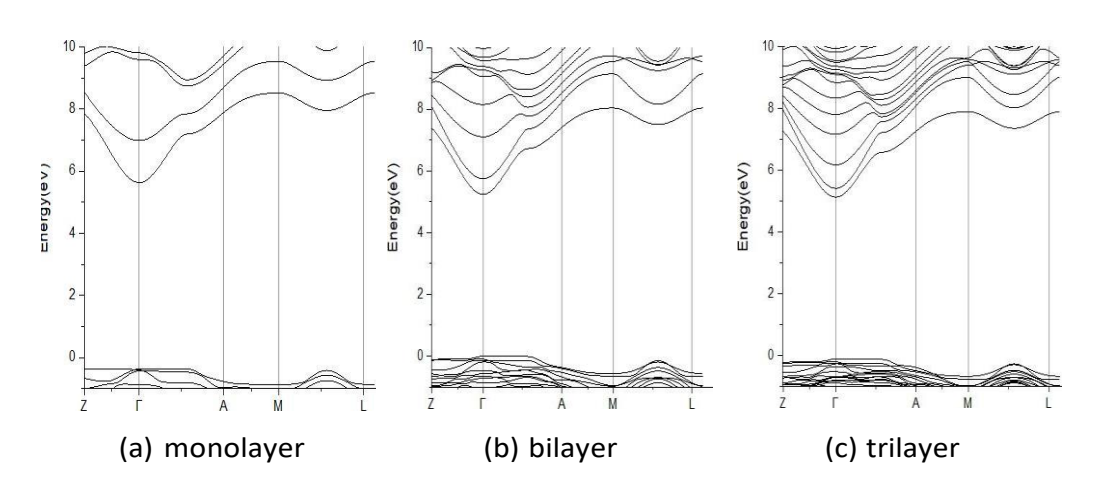


Figure 5.7: Band structures of layers

Table 5.2: Comparison Table

	direction	Effective mass of electron( $m^*/m_o$ )	Effective mass of holes( $m^*/m_o$ )
Bulk $\beta$ – $Ga_2O_3$		0.2895	17.04
monolayer	b	0.514	3.52
	С	0.551	55.32
bilayer	b	0.356	3.26
	С	0.258	62.23
trilayer	b	0.291	3.24
	С	0.236	50.82

The anisotropy of layers is observed from the above table indicating different effective mass along different directions. We can observe the valence band is almost flat indicating large effective mass for bulk and 2D layers of  $\beta$  – Ga2O3. Large effective mass of valence band gives us low hole mobility indicating the problem of p-type conductivity in  $\beta$  – Ga2O3.

We have oxygen and gallium oxygen vacancies in the bulk crystal  $\beta$  – Ga2O3. Since there are 3 different sites for O vacancy and 2 different sites for Ga as shown in Fig 2.4. This unit cell consists of 20 atoms of 8 gallium and 12 oxygen atoms.

One gallium atom and one oxygen atom is removed to create a vacancy at different sites respectively. The single vacancy have been created at different sites of oxygen in the unit cell Fig 5.8 and similarly done for gallium vacancy and the observed band structures are shown in Fig 5.9 and 5.10. It has been observed that O(III) site is the most stable site[31] and Ga(I) has lower formation energy[2], lower the formation energy more can be the concentration.

From the band structures we can observe the oxygen and gallium vacancies induce new levels in the valence band and conduction respectively. Gallium vacancies act as deep acceptors and oxygen vacancies act as deep donors as seen from the band structures.

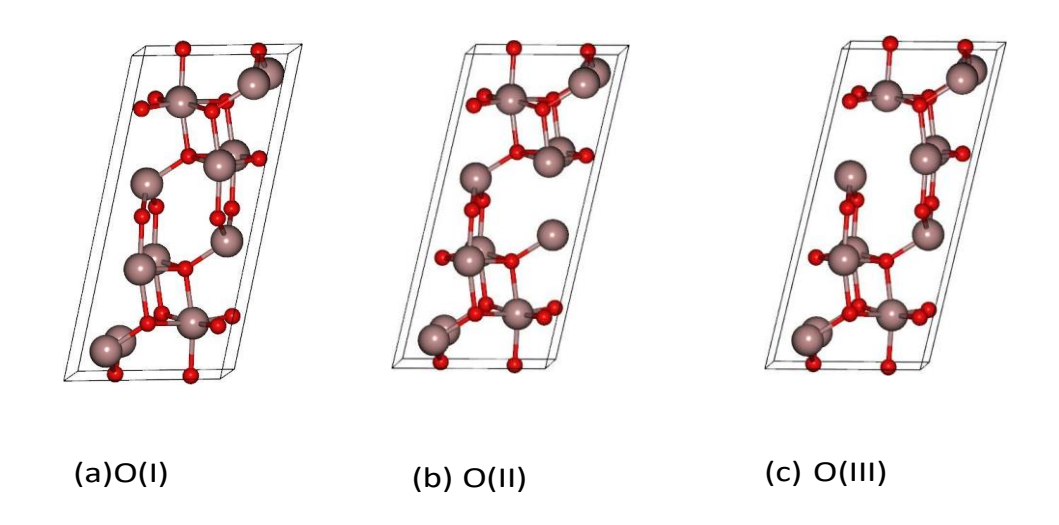


Figure 5.8: Oxygen vacancies in  $\theta - Ga_2O_3$ 

For doping, a 1x2x2 super cell  $\theta - Ga_2O_3$  consisting of 80 atoms of 32 gallium atoms and 48 oxygen atoms is considered. As mentioned Sn, Ir, Cr doping is done at the Ga(II) site while Si and Ge doping are done at Ga(I) sites as shown in Fig 5.11. All types of doping have been performed on 1x2x2 super cell. Only for the ease of view all are shown in the same Figure. Doping in the bulk crystal

Table 5.3: Band gap due to vacancies

	Band gap by	Band gap by
	DFT (eV)	using HSE06 (eV)
O(I)	0.6036	2.1982
O(II)	0.3252	1.852
O(III)	0.3168	1.667
Ga(I)	1.857	3.7934
Ga(II)	1.571	3.5264

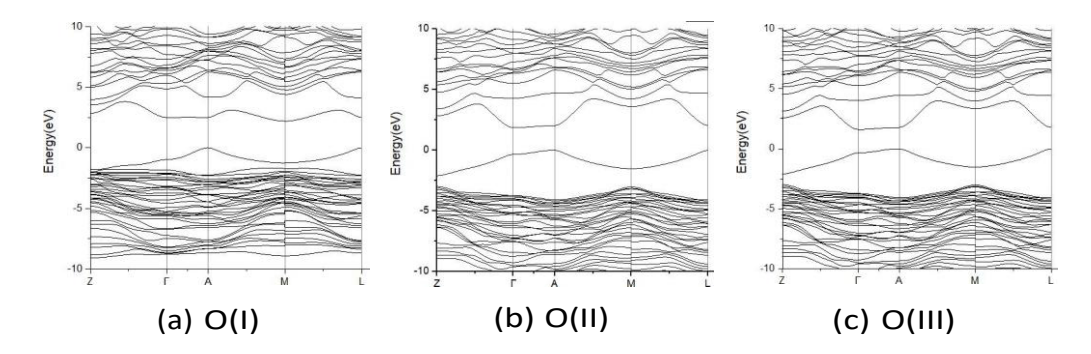


Figure 5.9: Band structures due to oxygen vacancies in  $\theta$  –  $Ga_2O_3$ 

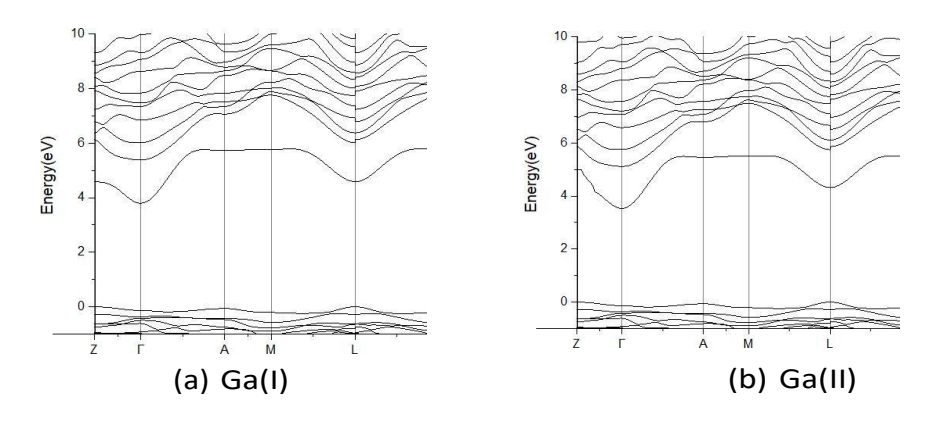


Figure 5.10: Band structures due to gallium vacancies in  $\theta$  –  $Ga_2O_3$ 

Group-IV elements which have extra valence electron than Gallium for n-type conductivity. We can observe here also new donor energy levels are induced below the conduction band edge.

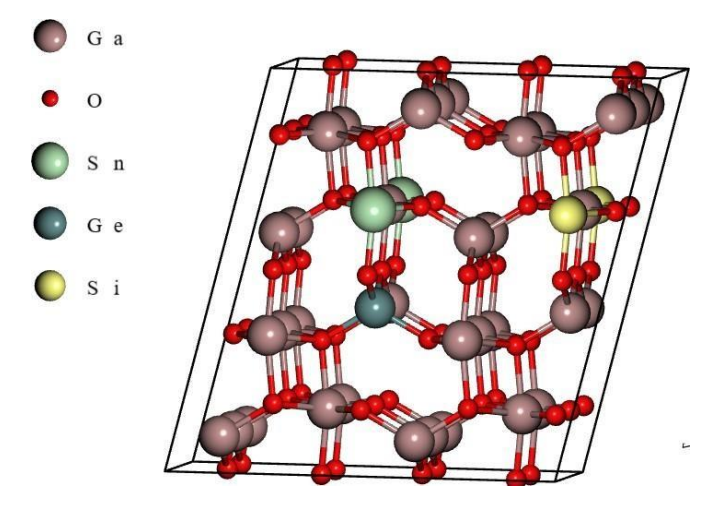


Figure 5.11: Doping in  $\beta - Ga_2O_3$ 

Table 5.4: Band gap

	Band gap by	Band gap by	effective mass
	DFT (eV)	using HSE06 (eV)	$m^*/m_o$
Si	2.112	4.8412	0.32
Ge	2.014	4.8361	0.278
Sn	2.009	4.8356	0.257
Ir	1.52	2.7453	0.268
Cr	1.478	2.212	0.221

The minimum amount of energy required to remove a loosely bound electron is called Binding energy  $E_d$  [3] or ionization energy. It is defined as the difference between the conduction band edge and the new level below the conduction band edge which should be less than 1eV to be a shallow donor.

From Fig 5.12 wecan observe Iridium and Chromium have deep donor levels in the band structure which sit on the Ga(II) site. Ir and Cr are transition elements so are capable of exhibiting variable valency. Iridium impurity incorporation occurs when bulk  $Ga_2O_3$  crystals are grown in an iridium crucible. From the band structure we observe that Chromium is in +3 state and acts as neutral donor with 3 bands

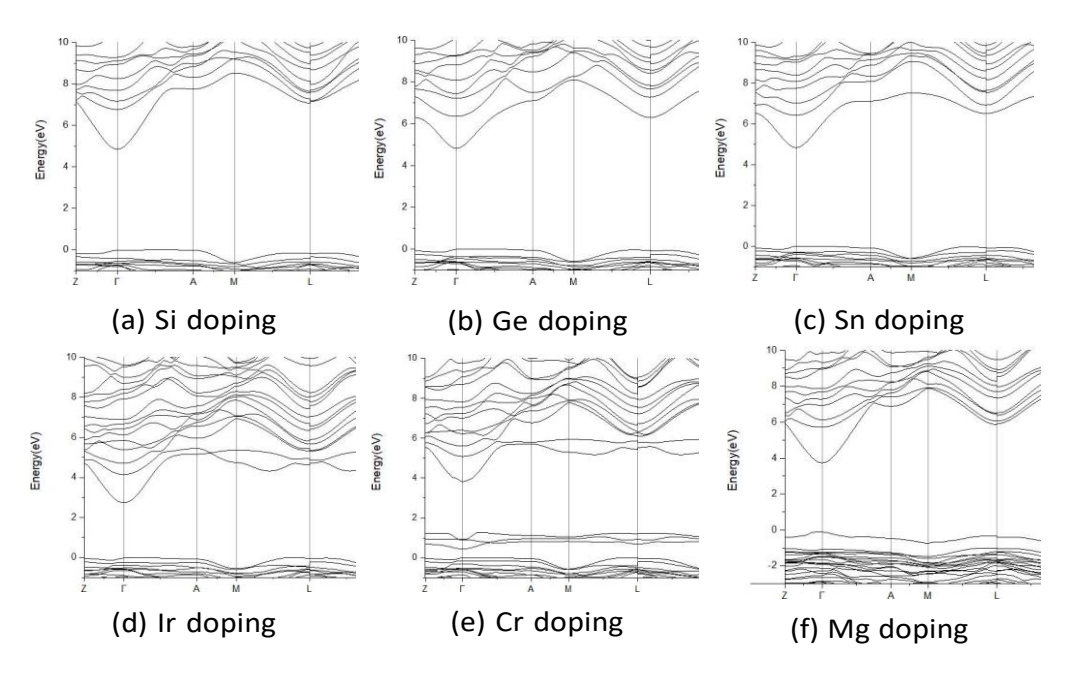


Figure 5.12: Band structures of different dopants in  $\theta$  –  $Ga_2O_3$ 

in between the band gap indicating we have filled mid-gap states of the neutral cell. There are new levels in both conduction and valence band of Cr. Ir in +4 valence will act as deep donor and +3 state as neutral donor.

Since Ir and Cr have  $E_d=2.09 \, \mathrm{eV}$  and 1.04eV indicating which require high ionization energy to ionize all the dopants, hence treated as deep donors for  $\beta-Ga_2O_3$ . Since deep donors does not contribute much for conduction and more concentration of dopants is required[36] since these act as active recombination sites and suitableat high temperature as dopants. Whereas the  $E_d$  values for Si, Ge, Sn are 41meV, 92meV, 97meV respectively indicating these all dopants behave like shallow donors for  $\beta-Ga_2O_3$ .

We can observe that Si behaves like a more shallow donor. It was observed that with moderate doping it generates free carrier concentration in  $\sim 10^{19}$  [3] and various experiments have shown Si is an unintentional source of n-type conductivity[2].

Mg doping on the Ga (II) is done for having p-type conductivity as it has one electron less than Gallium so can act as acceptor which shows a deep level in the valence band indicating it as a deep level acceptor with  $E_d = 1.1 \text{eV}$ . Many researchers have shown that various doping in  $\theta - Ga_2O_3$  has this type of deep level traps in the valence band, which require high concentrations of dopants and with flat valence band of holes the difficulty of getting p-type conductivity.

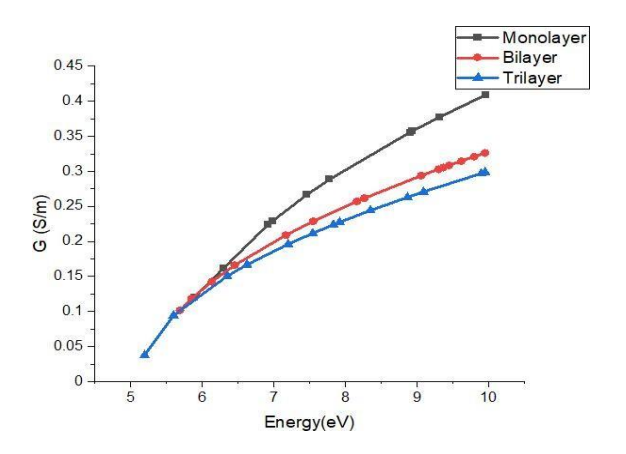


Figure 5.13: Conductance variation with energy in  $\theta$  –  $Ga_2O_3$  layers

The Fig 5.13 shows the variation of conductance as a function energy which has a parabolic relation for 2D  $\theta$  – $Ga_2O_3$  layers. The conductance is calculated by using Eq 4.22 and the number of sub bands by Eq 4.18, Eq 4.20 for the 2D and the bulk materials. The unit of conductance is V or Siemens(S). The number of modes M(E) is expressed as  $M_{2D}(E)/\mu m$ ,  $M_{2D}(E)/\mu m^2$  and conductance has the units  $S/\mu m$  and  $S/\mu m^2$  for 2D and the 3D bulk materials of  $\theta$  –  $Ga_2O_3$  respectively.

To get the exact the number of modes we can multiply the M(E) with the widthof 2D conductor or cross -sectional area of 3D conductor. From the Fig 5.13 for monolayer for a energy at 7eV calculated using Eq 4.18 is  $M_{2D}(E) = 2558.5/\mu m$ if the width of the conductor is 1nm then the number of channels for conductionare  $M_{2D}(E) \sim 2$ .

Similarly, we can find the channels contributing for conduction when the width or cross-sectional area of conductors is known. The Fig 5.14 shows variation of conductance for different doping concentrations with 3%, 15%, 25% (in atoms) for shallow donors Si, Ge, Sn and the deep donors Ir and Cr.

In case of Si, Ge, Sn when the doping concentration increases there is not much significant change in the band structure except in the concentration of free charge carriers in the conductance but in Ir and Cr have more deep levels and the binding energy changes significantly not like in the case of shallow donors.

Doping is done in the 1x2x2 super cell bulk  $\beta - Ga_2O_3$  and the conductance as function of energy has a linear relationship not like in 2D materials. This is true because as the size of the device increases it can accommodate more channels for conduction.

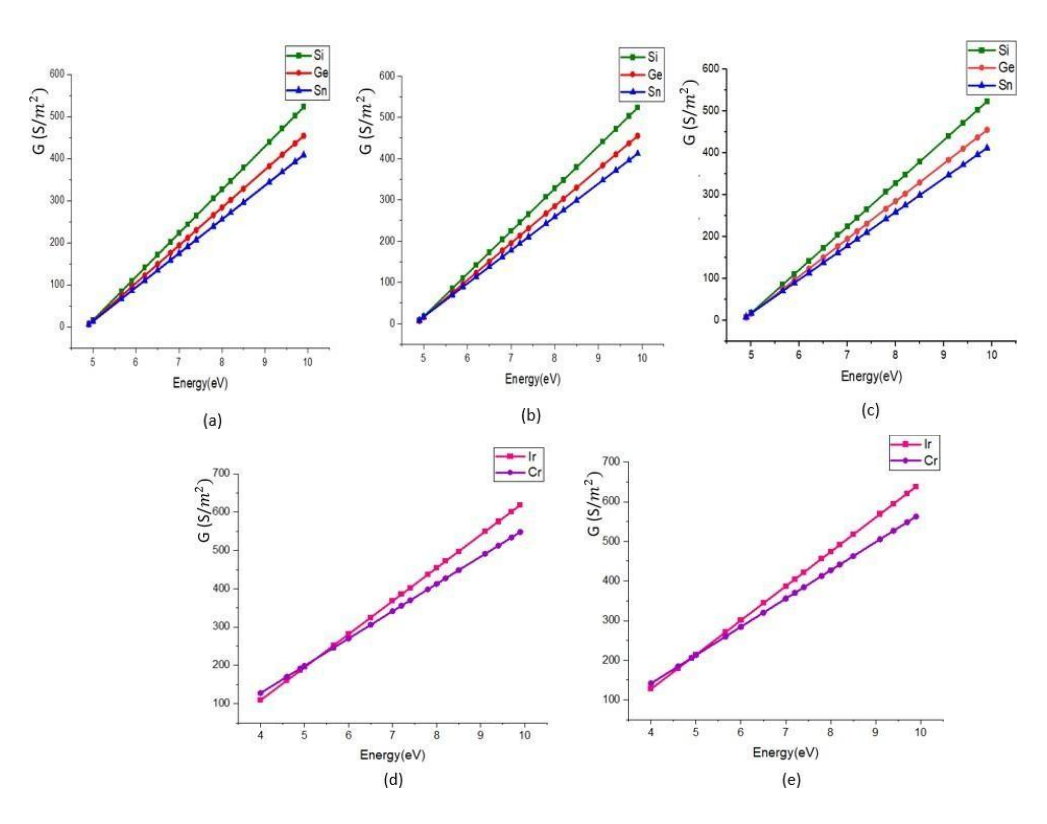


Figure 5.14: G variation with Energy for different concentration of doping in  $\beta - Ga_2O_3$ . For (a) 3% (b) 15% (c) 25% doping concentration in Si, Ge, Sn and (d)3% (e)15% doping concentration for deep donors Ir and Cr.

For each doping concentration the band gap and effective mass are calculated and the graphs are plotted for using Eq 4.22, Eq 4.20. The conductance unit of 3D materials is  $S/\mu m^2$  and similarly the number of channels can be found if we know the cross-sectional area of device.

# **Conclusion and Future Scope**

We know that the performance of 2D materials depends on the thickness hence, we observed thickness dependent band gap and effective mass variation due to the quantum confinement effect. From bulk 3D material by moving to 2D monolayer we have an increased band gap and monolayer possess highest band gap among all.

It was also observed that the low mobility issues had improved when moved to thin atomic layers than the bulk. The advantages of 2D materials is these layers are only few atoms thick, so are lighter and have very strong bonds so are difficult to break and can handle high voltages and high power without damaging the devices.

From ballistic conduction we can observe that the current density is not dependent on the length of semiconductor. We can get higher values of current density even if the channel length is made very small by moving from bulk to 2D layers of  $\theta - Ga_2O_3$ . Also, we can observe monolayer showing the maximum ballistic conductance, yielding a high current density with the minimum dimensions of the 2D  $\theta - Ga_2O_3$ .

The wide band gap semiconductors behave like an insulator. The calculated conductivity and mobility values are very less [7]. The large n-type conductivity values for gallium oxide were thought to be because of oxygen vacancies, but which is not true because the act as deep donors as seen from the band structure.

5.9. Gallium vacancies also do not contribute any n-type conductivity because they act as deep acceptors. As observed Si has lower ionization energy than Ge,Sn, Ir, Cr, Mg and has the highest ballistic current density with and can givehigh carrier concentration so, can be the best source for n-type conductivity of  $\theta - Ga_2O_3$ .

Materials doped with shallow level all the donors are nearly ionized ata moderate temperature on the other hand high ionization energy require higher temperatures to ionize the impurities so, deep donors may be suitable at higher temperatures but produce a smaller number of carriers compared to shallow donors at a given concentration.

From the valence band of band structures, we can say the effective mass is very high for p-type conductivity, which is indirectly related tomobility of holes so, it is difficult to have p type conductivity in gallium oxide.

Many theoretical calculations have shown the p-type conductivity with different dopants like Mg, N ,Fe have introduced deep acceptor levels and even with high concentrations of dopant it is impossible to get high mobility because of strong self-localisation of holes[30] and research is going on this.

Gallium oxide is a vast research topic and has good progress theoretically recently, because of the advantages of high band gap and high breakdown field strength for high voltage devices.

More progress can be done on improving the p- type conductivity of holes by observing it in different crystal orientations. Since the optical band gap value is nearly the electrical band gap and when doped with different materials give rise to new levels can be used for detection of variouswavelengths. So gallium oxide in the field of opto-electronics is a vast and ongoing topic for future direction[37].

Deep levels are useful when operated at higher temperatures so, more study can be done on deep donors when operated under suitable conditions.  $\alpha - Ga_2O_3$  has higher band gap than  $\theta - Ga_2O_3$  so further developments on this phase can be useful. More research can be done to investigate the use of other transition metal dopants like Cr and Ir which have more number of valence electrons so, can give high concentration of free carriers thereby increasing conductivity.

## References

- [1] B. Bayraktaroglu, "Assessment of gallium oxide technology," Air Force Research Labora-tory, Sensors Directorate WPAFB United States, Tech. Rep., 2017.
- [2] J. Zhang, J. Shi, D.-C. Qi, L. Chen, and K. H. Zhang, "Recent progress on the electronic structure, defect, and doping properties of  $ga_2o_3$ ," APL Materials, vol. 8, no. 2, p. 020906, 2020.
- [3] M. D. McCluskey, "Point defects in  $ga_2o_3$ ," Journal of Applied Physics, vol. 127, no. 10, p. 101101, 2020.
- [4] H. Zhou, J. Zhang, C. Zhang, Q. Feng, S. Zhao, P. Ma, and Y. Hao, "A review of the most recent progresses of state-of-art gallium oxide power devices," *Journal of Semiconductors*, vol. 40, no. 1, p. 011803, 2019.
- [5] R. Anvari, "Theoretical study of the  $ga_2o_3$ /electrolyte interface with application to gallium nitride heterostructure based chemical sensors," 2018.
- [6] W. Kohn, A. D. Becke, and R. G. Parr, "Density functional theory of electronic structure," *The Journal of Physical Chemistry*, vol. 100, no. 31, pp. 12 974–12 980, 1996.
- [7] J. Su, R. Guo, Z. Lin, S. Zhang, J. Zhang, J. Chang, and Y. Hao, "Unusual electronic and optical properties of two-dimensional  $ga_2o_3$  predicted by density functional theory," *The Journal of Physical Chemistry C*, vol. 122, no. 43, pp. 24592–24599, 2018.
- [8] J. Su, J. Zhang, R. Guo, Z. Lin, M. Liu, J. Zhang, J. Chang, and Y. Hao, "Mechanical and thermodynamic properties of two-dimensional monoclinic  $ga_2o_3$ ," *Materials & Design*, vol. 184, p. 108197, 2019.
- [9] Y. Liao, Z. Zhang, Z. Gao, Q. Qian, and M. Hua, "Tunable properties of novel ga2o3 monolayer for electronic and optoelectronic applications," *ACS applied materials & interfaces*, vol. 12, no. 27, pp. 30 659–30 669, 2020.

- [10] J. Kim, M. A. Mastro, M. J. Tadjer, and J. Kim, "Quasi-two-dimensional h-bn/β-ga2o3 heterostructure metal–insulator–semiconductor field-effect transistor," ACS applied materials & interfaces, vol. 9, no. 25, pp. 21322–21327, 2017.
- [11] P. E. Blöchl, "Projector augmented-wave method," *Physical review B*, vol. 50, no. 24, p. 17953, 1994.
- [12] G. Kresse and D. Joubert, "From ultrasoft pseudopotentials to the projector augmented-wave method," *Physical review b*, vol. 59, no. 3, p. 1758, 1999.
- [13] L. Dong, R. Jia, B. Xin, B. Peng, and Y. Zhang, "Effects of oxygen vacancies on the structural and optical properties of  $\beta$   $ga_2o_3$ ," Scientific reports, vol. 7, no. 1, pp. 1–12, 2017.
- [14] P. Deák, M. Lorke, B. Aradi, and T. Frauenheim, "Optimized hybrid functionals for defect calculations in semiconductors," *Journal of Applied Physics*, vol. 126, no. 13, p. 130901, 2019.
- [15] G. Ramalingam, P. Kathirgamanathan, N. Manivannan, and K. Kasinathan, "Quantum confinement effect of 2d nanomaterials," in *Quantum Dots-Fundamental and Applications*. IntechOpen, 2020.
- [16] L. Alvarez, "Introduction of the concepts of hole and effective mass using an alternative to the e-k diagram," *Revista mexicana de física E*, vol. 59, no. 2, pp. 128–132, 2013.
- [17] J. Bardeen and W. Shockley, "Deformation potentials and mobilities in non-polar crystals," *Physical review*, vol. 80, no. 1, p. 72, 1950.
- [18] M. Higashiwaki, K. Sasaki, A. Kuramata, T. Masui, and S. Yamakoshi, "Gallium oxide ( $ga_2o_3$ ) metal-semiconductor field-effect transistors on single-crystal  $\beta$   $ga_2o_3$  (010) sub- strates," Applied Physics Letters, vol. 100, no. 1, p. 013504, 2012.
- [19] J. L. Hudgins, G. S. Simin, E. Santi, and M. A. Khan, "An assessment of wide bandgap semiconductors for power devices," *IEEE Transactions on Power Electronics*, vol. 18, no. 3, pp. 907–914, 2003.
- [20] E. Kohn and A. Denisenko, "Concepts for diamond electronics," *Thin Solid Films*, vol. 515, no. 10, pp. 4333–4339, 2007.

- [21] R. Roy, V. Hill, and E. Osborn, "Polymorphism of  $\beta ga_2o_3$  and the system  $\beta ga_2o_3 h_2o$ ," Journal of the American Chemical Society, vol. 74, no. 3, pp. 719–722, 1952.
- [22] E. Chikoidze, H. Von Bardeleben, K. Akaiwa, E. Shigematsu, K. Kaneko, S. Fujita, and Y. Dumont, "Electrical, optical, and magnetic properties of sn doped  $a-ga_2o_3$  thin films," *Journal of Applied Physics*, vol. 120, no. 2, p. 025109, 2016.
- [23] H. He, R. Orlando, M. A. Blanco, R. Pandey, E. Amzallag, I. Baraille, and M. Rérat, "First-principles study of the structural, electronic, and optical properties of  $ga_2o_3$  in its monoclinic and hexagonal phases," *Physical Review B*, vol. 74, no. 19, p. 195123, 2006.
- [24] M.-G. Ju, X. Wang, W. Liang, Y. Zhao, and C. Li, "Tuning the energy band-gap of crys-talline gallium oxide to enhance photocatalytic water splitting: mixed-phase junctions," *Journal of Materials Chemistry A*, vol. 2, no. 40, pp. 17005–17014, 2014.
- [25] F. Elsholz, "Landauer büttiker formalism," *Univesity of Rochester, Rochester, NY, USA*, 2002.
- [26] M. Z. Diešková, A. Ferretti, and P. Bokes, "Tunneling through al/alo x/al junction: Analytical models and first-principles simulations," *Physical Review B*, vol. 87, no. 19, p. 195107, 2013.
- [27] M. Baldo, Introduction to nanoelectronics, Part 4. MIT OpenCourseWare, 2011.
- [28] G. Ramalingam, P. Kathirgamanathan, N. Manivannan, and K. Kasinathan, "Quantum confinement effect of 2d nanomaterials," in *Quantum Dots-Fundamental and Applications*. IntechOpen, 2020.

- [29] V. Bermudez, "The structure of low-index surfaces of  $ga_2o_3$ ," Chemical Physics, vol. 323, no. 2-3, pp. 193–203, 2006.
- [30] A. Kyrtsos, M. Matsubara, and E. Bellotti, "On the feasibility of p-type  $ga_2o_3$ ," Applied Physics Letters, vol. 112, no. 3, p. 032108, 2018.
- [31] J. B. Varley, J. R. Weber, A. Janotti, and C. G. Van de Walle, "Oxygen vacancies and donor impurities in  $ga_2o_3$ ," Applied Physics Letters, vol. 97, no. 14, p. 142106, 2010.
- [32] B. I. Shklovskii and A. L. Efros, *Electronic properties of doped semiconductors*. Springer Science & Business Media, 2013, vol. 45.
- [33] M. J. Tadjer, J. L. Lyons, N. Nepal, J. A. Freitas Jr, A. D. Koehler, and G. M. Foster, "Review—theory and characterization of doping and defects in -B  $ga_2o_3$ ," ECS Journal of Solid State Science and Technology, vol. 8, no. 7, p. Q3187, 2019.
- [34] R. Ahrling, J. Boy, M. Handwerg, O. Chiatti, R. Mitdank, G. Wagner, Z. Galazka, and S. F. Fischer, "Transport properties and finite size effects in  $\mathcal{B}$   $ga_2o_3$  thin films," Scientific reports, vol. 9, no. 1, pp. 1–9, 2019.
- [35] S. Marcinkevičius and J. S. Speck, "Ultrafast dynamics of hole self-localization in  $\beta$   $ga_2o_3$ ," Applied Physics Letters, vol. 116, no. 13, p. 132101, 2020.
- [36] Q. Song, J. Zhou, L. Meroueh, D. Broido, Z. Ren, and G. Chen, "The effect of shallow vs deep level doping on the performance of thermoelectric materials," *Applied Physics Letters*, vol. 109, no. 26, p. 263902, 2016.
- [37] D. Guo, Q. Guo, Z. Chen, Z. Wu, P. Li, and W. Tang, "Review of  $ga_2o_3$ -based optoelectronic devices," *Materials Today Physics*, vol. 11, p. 100157, 2019.